Physics – Uspekhi **65** (3) 227 – 244 (2022)

REVIEWS OF TOPICAL PROBLEMS

PACS numbers: **61.46. – w,** 64.70.P – , **64.75. – g**

Nanocrystal formation in homogeneous and heterogeneous amorphous phases

G E Abrosimova, D V Matveev, A S Aronin

DOI: https://doi.org/10.3367/UFNe.2021.04.038974

Contents

Abstract. This review describes the current state of research on the formation of a nanocrystalline structure in amorphous alloys under thermal and deformation effects. The processes of formation of nanocrystals in homogeneous and heterogeneous amorphous structures (nanoglass) are considered. Changes in the magnetic and mechanical properties during the formation of a composite amorphous-nanocrystalline structure with different structural parameters are analyzed. The possibility of amorphous phase rejuvenation from a partially crystalline structure under cryogenic thermocycling treatment is shown.

Keywords: nanocrystals, metallic glasses, heterogeneous amorphous structure, nanoglass, crystallization, phase transformation

1. Introduction

Nanostructures are one of the most widely studies objects, since they underlie the creation of new materials, possessing a combination of remarkable and, in many cases, unique physical properties. Nanostructures can be obtained by different methods, such as sputtering, low-energy grinding [1], sintering of powders, and thermal treatment or deformation of the amorphous phase (rolling [2, 3], bending deformation [4], etc.). The most widespread methods are those of producing a nanostructure from the amorphous phase by thermal treatment [5–13] and intense plastic deformation (high pressure torsion) [14–19]. Studies have shown that the parameters of the resulting nanostructure substantially depend on the chemical composition and conditions of the external action (temperature, duration of heating or annealing, deformation rate and magnitude, etc.) [20–22]. A structural change naturally affects the material properties. In the present review, we consider the principles of fabricating metallic nanostructures, the dependence of their parameters on the external action conditions, and the correlation between the material structure and properties.

G E Abrosimova [(a)], **D V Matveev** [(b)], **A S Aronin** [(c)]
Institute of Solid State Physics, Russian Academy of Sciences,
ul. Akademika Osip'yana 2, 142432 Chernogolovka, Moscow region,
Russian Federation
E-mail: [(a)]gea@issp.ac.ru, [(b)]matveev@issp.ac.ru, [(c)]aronin@issp.ac.ru

Received 3 November 2020, revised 15 March 2021
Uspekhi Fizicheskikh Nauk **192** (3) 247 – 266 (2022)
Translated by V L Derbov

2. Processes of solidification and crystallization

When speaking about the structure of solids, several groups are usually considered: single crystals, polycrystals, quasicrystals, nanocrystals, amorphous materials, and nanoglasses. The first two have been known for more than a century; quasicrystals were discovered in 1094 when studying Al–Mn alloys [23] and have since been observed in many systems [24–28]. In contrast to crystals, quasicrystals are nonequilibrium structures. Amorphous alloys (or metallic glasses) and nanoglasses (heterogeneous metallic glasses) are also nonequilibrium structures; like quasicrystals, they are obtained by fast quenching of a melt on a rapidly moving substrate. Metallic glasses were first obtained in 1960 [29], and the understanding of the fact that they can be heterogeneous appeared much later. Although the heterogeneous structure of amorphous alloys was observed by many researchers [30–36], the term 'nanoglasses' appeared only in 2013 in a paper by Gleiter [37]. It is interesting to note that both natural and artificial solids are formed, generally, in a similar way: crystalline ones through relatively slow processes, and amorphous ones under fast exposures. Simple examples are as follows: slowly formed stalactites (chemogenic sinter formations of calcites in karst caves) and stalagmites (mineral sinter formations) are crystalline, and fulgurites (the sand SiO_2 sintered by a lightning blow) are

amorphous [38]. As metallic glasses formed under the cooling of a melt at a rate of about 10^6 K s^{-1}, fulgurite forms under the action of vapors of instantly boiled moisture between grains of sand followed by fast cooling.

Nanostructures obtained through amorphous phase crystallization, in fact, are composite amorphous-crystalline materials and consist of nanometer-sized crystals separated from each other by an amorphous layer. Such a structure forms in the process of amorphous phase crystallization and, naturally, substantially depends on the crystallization conditions. Amorphous phase crystallization processes have been studied in various systems; in this case, homogenic crystal nucleation in the amorphous phase [39], heterogeneous nucleation [40, 41], or spinodal decomposition [36, 42–44] were observed. Under heating, nanocrystalline structures commonly appear as a result of the primary crystallization reaction.

2.1 Formation of nanocrystals in a homogeneous amorphous phase

Crystallization of the amorphous phase (like that of a melt) usually occurs through the nucleation and growth of crystals. The driving force of the crystallization process is the difference in free energy between the liquid and glassy phases ΔG. The value of ΔG can be calculated from the melting enthalpy ΔH and overcooling $\Delta T = T - T_m$ (T_m being the melting temperature). The expression for ΔG can with some approximation be written as [45]

$$\Delta G = \frac{\Delta H \Delta T}{T_m} \frac{2T}{T_m + T} . \tag{1}$$

Depending on composition, the crystallization occurs as a result of a primary (or preferential), polymorphic, or eutectic reaction [46–49]. A polymorphic transformation results in the formation of one crystal phase having the same composition as the amorphous phase (or melt). In the primary crystallization, a single phase forms, too, but its composition differs from that of the amorphous phase. A eutectic crystallization leads to the simultaneous appearance of two phases which can form colonies with certain orientation interrelations between lattices of crystallizing phases.

Upon nucleation of a spherical crystal in an amorphous phase, the free energy change is described by the equation

$$\Delta G = -\frac{4}{3}\pi r^3 \frac{\Delta G_0}{V_m} + 4\pi r^2 \gamma , \tag{2}$$

where ΔG_0 is the gain in free energy per mole during the transformation of glass into a crystal, r is the radius of the nucleus, V_m is the molar volume, and γ is the interfacial energy.

The critical radius r^* is evaluated using the position of the ΔG curve maximum:

$$r^* = \frac{2\gamma V_m}{\Delta G_0} . \tag{3}$$

The free energy barrier height, associated with the formation of a nucleus of the critical size, can be found from the following equation:

$$\Delta G_c = \frac{16\pi}{3} \frac{\gamma^3}{\Delta G_0^2} V_m . \tag{4}$$

In the nucleation theory, it is usually assumed that the steady-state concentration of nuclei or clusters always exists. However, at the very beginning, there must be a finite period of time during which the steady-state distribution of nuclei is established [50]. There is a certain time during which the steady-state distribution of clusters, corresponding to the classical theory, is achieved. The time-dependent rate of formation of crystallization centers $I(t)$ obeys the equation [51]

$$I(t) = I_{st}\left[1 + 2\sum_{n=1}^{\infty} (-1)^n \exp\left(-n^2 \frac{t}{\tau}\right)\right] , \tag{5}$$

where τ is the incubation period, which greatly increases with a decrease in temperature, and I_{st} is the nucleation rate under steady-state conditions, which, in turn, is described by the equation [49]

$$I_{st} = I_0 \exp\left(-\frac{L\Delta G_c}{RT}\right) \exp\left(-\frac{Q_N}{RT}\right) , \tag{6}$$

L is the Loschmidt number, Q_N is the activation energy of passing an atom through the crystallization front, and ΔG_c is the free energy required to form a nucleus.

The preexponential factor usually varies from 10^{30} to 10^{35} nuclei cm^{-3} and depends on the specificity of the theory used [49].

The nucleation of crystals can occur according to a homogeneous of heterogeneous mechanism. Homogeneous nucleation occurs through fluctuation formation of a nucleus with a radius greater than the critical one. Homogeneous and heterogeneous nucleation often combine, for example, on 'frozen-in' crystallization centers (hardened clusters present in a melt immediately before cooling). Below the vitrification temperature, homogeneous nucleation requires too much time, and the nucleation caused by 'frozen-in' crystallization centers is of major importance for crystallization.

The rate of crystallization nuclei growth depends on the rate of atomic sedimentation on the surface of stable nuclei. The crystal growth rate u equals the difference between the probability of finding an atom with sufficient energy, which can leave the amorphous phase and join the crystal (Boltzmann statistics), and the probability of the back transition of the atom from the crystal to the amorphous phase [52]:

$$u = u_0 \exp\left(-\frac{Q_g}{RT}\right)\left[1 - \exp\left(-\frac{\Delta g}{RT}\right)\right] , \tag{7}$$

where the preexponential factor u_0 is determined by the relation

$$u_0 = a_0 v_0 , \tag{8}$$

a_0 is the atomic diameter, v_0 is the frequency of atomic jumping. The value of u_0 is known to be approximately 10^3 m s^{-1}. The activation energy Q_g is of the same order of magnitude as the activation energy of grain boundary diffusion.

In the crystallization of metallic glasses, the situation when the temperature is much lower than the melting temperature T_m is of particular interest. In this case, $\Delta g \gg RT$ and the value of $\exp(-\Delta g/RT)$ is small. Therefore, in the case of strong overcooling, the growth rate will obey the Arrhenius-

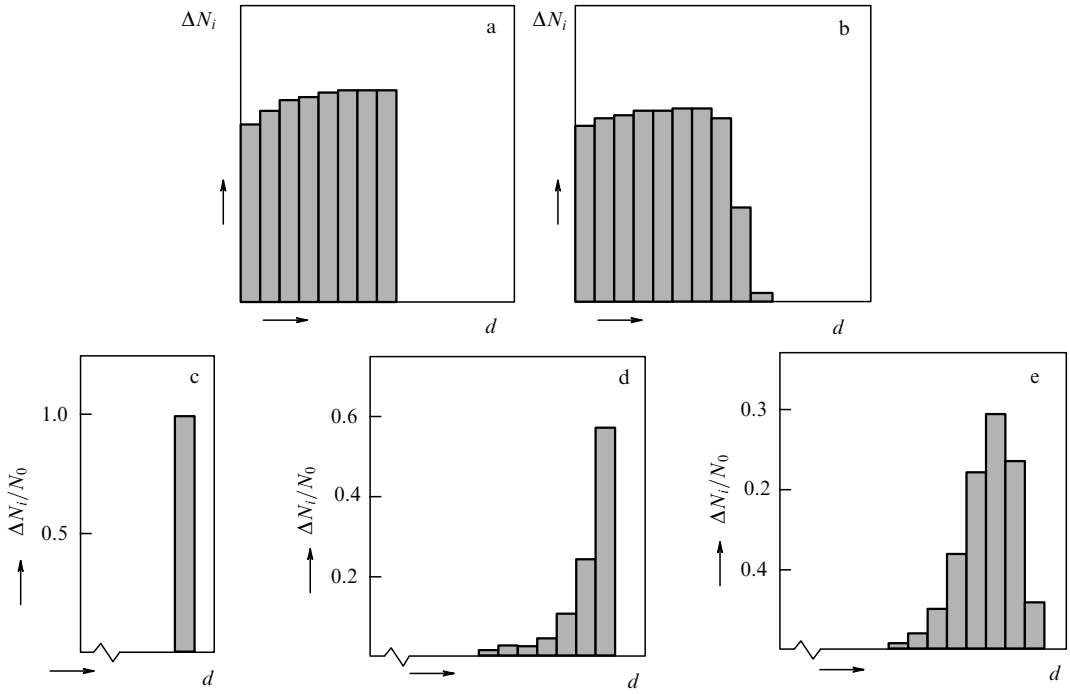

Figure 1. Histograms of size distribution of grains for homogeneous (a, b) and heterogeneous (c–e) nucleation, (b, d, e) being cases of unestablished nucleation. ΔN_i is the number of crystals of a given size, N_0 is the total number of crystals.

type equation

$$u \approx u_0 \exp\left(-\frac{Q_g}{RT}\right). \tag{9}$$

According to this mechanism, the grains will grow until they begin to contact each other.

Crystal growth depends on the type of transformation and can proceed linearly or parabolically [53]. The size distribution of the crystals for different growth laws is presented in Fig. 1 [53].

Distributions (a, b) correspond to homogeneous nucleation, the rest, to heterogeneous nucleation. Distributions b, d, e correspond to the case of not yet established nucleation. It is known that linear growth is characteristic of the transformations that occur without the composition change (polymorphic reactions) or combined transformations, when the mean composition of the crystalline region corresponds to the matrix composition (eutectic reactions). Parabolic growth is mainly characteristic of the reactions controlled by volume diffusion, i.e., those of primary crystallization [51]. In this case, it should be taken into account that the change in the concentrations of the components in the surrounding matrix should be insignificant, i.e., the parabolic growth should be characteristic of the initial stages of crystallization.

During the primary crystallization, when the growth of a crystal is controlled by volume diffusion, the time dependence of the crystal size is described by the formula

$$r = \alpha(Dt)^{1/2}, \tag{10}$$

where D is the diffusion coefficient, and α is a constant (a dimensioned parameter determined from the composition of the boundary region of the particle and the sample composition) representing so-called supersaturation, which will be considered below [47, 51, 53–55]. It is commonly accepted that the diffusion coefficient D is independent of concentration. Its temperature dependence is given by the Arrhenius-type expression

$$D = D_0 \exp\left(-\frac{Q_D}{RT}\right). \tag{11}$$

The crystal growth rate u_p during primary crystallization obeys the equation

$$u_p = \frac{dr}{dt} = \frac{\alpha}{2}\left(\frac{D}{t}\right)^{1/2}. \tag{12}$$

According to multiple data, the activation energy of crystal expulsion in the amorphous phase amounts to 145–250 kJ mol^{-1}. Since the activation energy of self-diffusion of metallic atoms in a crystal is ≈ 250 kJ mol^{-1}, and the activation energy of diffusion of a as carbon metalloid such is 125–145 kJ mol^{-1}, the activation energy of the diffusion of amorphous phase atoms is expected to be somewhat lower than in the crystalline phase.

The specific features of crystal formation in the amorphous phase have been studied in many systems [40, 56–59]. One example of such studies is the analysis of primary crystallization in amorphous alloys of the Fe–B system [60]. The authors of Ref. [60] proposed a model of the primary crystallization kinetics, namely, of the formation of α-Fe crystals in the amorphous phase. The model is based on the approximate solution of the balance equation for the steady-state flow taking into account the soft action of diffusion fields of the growing crystals, as well as on the Kolmogorov–Johnson–Mehl–Avrami formalism. The authors showed that the model correctly describes the behavior of nanocrystals in the process of primary crystallization, in particular, the experimentally observed decrease in the Avrami index, and obtained good agreement of the calculated diffusion coefficient values with the appropriate experimental data.

As in Ref. [61], to describe diffusion-limited crystal growth with the effect of the overlap of diffusion fields taken into

account, the authors of Ref. [60] used the balance equation for a steady-state flow,

$$\frac{\mathrm{d}R(t)}{\mathrm{d}t} = \frac{C_\mathrm{I} - C_\mathrm{m}(t)}{C_\mathrm{I} - C_\mathrm{p}} \frac{D}{R(t)}, \tag{13}$$

and the law of conservation of diluted components,

$$\frac{4\pi}{3}(C_\mathrm{p} - C_\mathrm{I})\left[R^3(t) - R^3(0)\right] = \frac{4\pi}{3} R_\mathrm{s}^3 \left[C_\mathrm{m}(0) - C_\mathrm{m}(t)\right], \tag{14}$$

where C_p is the concentration of the component dissolved in the particle, C_I is the concentration in the matrix at the interface between particles, $C_\mathrm{m}(0)$ and $C_\mathrm{m}(t)$ are the initial and time-dependent mean concentrations in the matrix, respectively, $R(0)$ and $R(t)$ are the initial and time-dependent radius of a particle, respectively, $2R_\mathrm{s}$ is the separation between particles, and D is the volume diffusion coefficient.

It is also worth noting that, for the growth of one crystal in an infinite matrix ($C_\mathrm{m}(t) \equiv C_\mathrm{m}(0)$ and $R(0) = 0$), the solution to Eqn (13) is the well-known solution of the Zener equation (Eqn (10)) for parabolic growth [62]. The exact solution to Eqns (13) and (14) obtained by Ham [61] is too cumbersome and inconvenient for practical use. It is also clear that the diffusion-controlled growth at early stages of primary crystallization corresponds to Eqn (3) and the contact of diffusion fields of adjacent particles (soft touch) can hamper growth only at the final stage of crystallization. Therefore, it is possible to use the approximate solution to the above system of equations in a form convenient for describing the decrease in the growth rate due to $C_\mathrm{m}(t) \to C_\mathrm{I}$ for the case where the mean concentration in the matrix is close to the concentration near the interface between particles. If $C_\mathrm{m}(0)$ is close to C_I and $R(0) \ll R_\mathrm{s}$, then the expression for estimating the change in the crystal radius with time at the final stage of the primary crystallization is

$$R(t) = \left\{ R^2(0) + \frac{2}{3} R_\mathrm{s}^2 \alpha^2 \left[1 - \exp\left(-\frac{3\alpha D t}{R_\mathrm{s}^2} \right) \right] \right\}^{1/2}, \tag{15}$$

under the assumption that $R_\mathrm{fin} \gg R(0)$ is simplified to

$$R_\mathrm{H}(t) \approx \sqrt{\frac{2}{3}} \alpha R_\mathrm{s} \left[1 - \exp\left(-\frac{3\alpha D t}{R_\mathrm{s}^2} \right) \right]^{1/2}. \tag{16}$$

Here, R_H is the Ham radius. It should be noted that, for the case $R_\mathrm{s} \to \infty$, Eqn (16) turns into Eqn (10), which confirms the correctness of the analysis carried out.

The comparison of calculations with the experimental data carried out by the authors of Ref. [60] showed that the approximate solution somewhat overestimates the value of R at the initial stage (by up to 10%) and underestimates (by up to 6%) it at the final stage of transformation compared to the numerical (accurate) analysis. The results of Refs [60, 63, 64] show that the entire process of primary crystallization can be divided into two stages. However, taking into account that the volume fraction of the crystallized phase and the free diffusion-controlled crystal growth (Eqn (10)) at the initial stage of transformation are relatively small (because of the small sizes of the growing crystals) compared to those formed at the final stage, when the diffusion fields touch each other (Eqn (16)), the change in the volume fraction of the crystallized material can be described by a simple kinetic equation based on the Kolmogorov–Johnson–Mehl–Avrami model [51]:

$$X(t) \approx 1 - \exp\left[-\frac{4\pi}{3} N_+ R_\mathrm{H}^3(t) \right], \tag{17}$$

where N_+ is the volume density of crystals nucleated at the early stage of transformations.

Later, this approach was used to describe not only the primary crystallization but also the later stages of crystallization in various alloys [65–67], with the results of differential scanning calorimetry or electric resistance measurement used as actual data to determine the fraction of the forming crystalline phase.

To clarify the mechanisms of crystal nucleation in the amorphous phase and to determine the characteristics of the crystallization process, it is possible to use the construction of size distributions of the crystals and an analysis of variations in these distributions with time. When applying such an approach to an aluminum-based amorphous alloy ($Al_{86}Ni_{11}Yb_3$) the authors of Ref. [68] showed that, in the process of annealing, the amorphous phase crystallization is implemented through heterogeneous nucleation with an incubation period. This conclusion was based on an analysis of the distributions obtained for different annealing times and showed a significant decrease in the region of small sizes at the initial stage of annealing, the absence of small crystals in the distribution after aging, and a gradual increase in the proportion of large particles upon increasing the aging time.

Heterogeneous nucleation at the early stages of crystallization of metallic glasses is the most frequent mechanism of crystallization. The sites of heterogeneous nucleation can be sample surfaces, internal imperfections, empty or gas-filled pores (during hardening, the melt is pressed out of an ampule by the excess pressure of a gas, as a rule, argon), or the so-called frozen out centers of crystallization (ordered regions, e.g., aggregates of one and the same kind of atoms). In particular, this is the foundation of the approach that allowed producing the first nanocrystalline alloy with the composition $Fe_{73.5}Si_{13.5}B_9Nb_3Cu_1$, later called Finemet [69]: the nucleation of nanocrystals in it occurs in the copper clusters, insoluble in the amorphous phase of this composition.

The formation of a nanocrystalline structure in the amorphous phase usually occurs according to the primary crystallization mechanism. In this case, the composition of nanocrystals differs from that of the amorphous alloy, i.e., the process of crystal formation is controlled by the volume diffusion. In the process of crystallization of the amorphous alloy with the base composition Fe–Si–B, depending on the concentration of components, the formation of either α-Fe crystals or eutectic colonies composed of α-Fe(Si) and Fe_3B occurs, but in either case the forming crystals grow very rapidly and no nanostructure appears. It is clear that for the formation of nanosize crystals it is necessary to ensure a high rate of crystal nucleation and a low rate of their growth. To achieve such conditions, small amounts of copper (1 at.%) and niobium (3 at.%) were introduced into the base Fe–Si–B composition. Since copper does not dissolve in iron, the copper clusters served as sites for nucleation of crystals, and the niobium atoms characterized by a low diffusion rate hampered the diffusive redistribution of components, giving rise to a low growth rate for the crystals forming in the amorphous matrix. It important to note that copper clusters

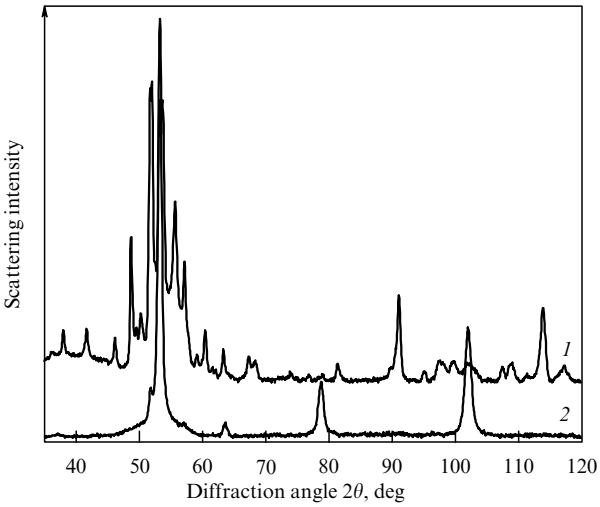

Figure 2. X-ray patterns of annealed alloys of the Co–Fe–Si–B–Nb system (*1* — $Co_{71.6}Fe_7Si_{12.4}B_9$, *2* — $Co_{70}Fe_7Si_{12}B_9Nb_2$).

are only regions of facilitated nucleation, but are by no means related structurally to the nucleating crystals. Copper is known to have a face-centered cubic (fcc) lattice, while the nanocrystals formed in the iron-based alloy have a body-centered cubic (bcc) lattice. Therefore, the nucleation of crystals on copper clusters reflects the difference in energy gain upon the heterogeneous nucleation of a crystal on a cluster (inhomogeneity) compared to a homogeneous nucleation of a crystal in the bulk of an amorphous matrix.

In recent years, a different approach has been developed, according to which the sites for nucleation of nanocrystals can be the regions of short-range order, packed according to the type of first crystallizing phase. For iron-based alloys, they should be regions packed according to the type of bcc structure. The prerequisites for such consideration are a number of factors:

— the short-range order in an amorphous phase can change, depending on the composition [70, 71] and/or temperature [72, 73];

— at the initial stage of amorphous alloy crystallization, in most cases, the crystal phases formed have a structure and composition close to the short-range order and the composition of the amorphous phase immediately before the beginning of crystallization ('inheriting' of the structure) [74], these phases being mostly metastable [75–78];

— in the process of amorphous phase separation (formation of a heterogeneous amorphous phase consisting of several amorphous phases), each of the amorphous regions crystallizes independently of the others, with the formation of its 'own' crystalline phase [79].

The possibility of forming bcc nanocrystals upon doping with bcc structure components in alloys whose main metallic component has a different lattice was studied in Refs [80, 81]. Figure 2 presents X-ray patterns of alloys of the Co–Fe–Si–B–N system, containing 0 (curve *1*) and 2 (curve *2*) at.% of Nb.

In the papers cited above, it was found that the introduction of 1–2 at.% of Nb (an element with a bcc lattice) into a cobalt-based alloy (fcc or hexagonal close-packed (hcp) lattice depending on temperature) facilitates the formation of bcc nanocrystals. Adding niobium to amorphous Co-based alloys not only gives rise to a structure not typical of alloys with the compositions studied, but also substantially affects the size of nanocrystals. In this case, as a result of doping, a crystal phase is formed with a lattice related to the structure of the doping element rather than the main component of the alloy. Studies carried out on this and other systems have shown that the presence of ordered regions in the amorphous phase facilitates the nucleation of nanocrystals with a lattice having the same short-range order as the ordered region. The crystals formed in the amorphous phase have a structure that differs from that of the main metallic component of the alloy [82]. The studies described are presently being continued.

2.2 Formation of nanocrystals in a heterogeneous amorphous phase

As was noted above, the formation of nanocrystals in amorphous alloys can occur through different mechanisms. The structure that forms depends on the chemical composition of the alloy, temperature, the method of acting on the structure, as well as on the state of the amorphous phase (homogeneous or heterogeneous) before the beginning of crystallization. Below, we consider the formation of a heterogeneous amorphous structure and some examples of nanostructure formation in nanoglasses.

2.2.1 Formation of a heterogeneous amorphous phase (nanoglass). The main method of investigating the structure of amorphous alloys is X-ray diffraction analysis. The intensity of scattering of X-rays by an amorphous phase is determined by the formula

$$I(S) = NF^2(S)\left\{1+\int_0^\infty 4\pi R^2\left[\rho(R)-\rho_0\right]\frac{\sin(SR)}{SR}\,\mathrm{d}R\right\}, \tag{18}$$

where N is the total number of atoms in a unit volume, $F(S)$ is the scattering amplitude, $\rho(R)$ is the number of atoms per unit volume at distance R from the chosen atom, ρ_0 is the mean number of atoms per unit volume, and S is the wave vector [83]. The sequence of maxima of function $I(S)$ is determined by the sequence of maxima of function $\sin(SR)/SR$. Since it has maxima at SR values of 7.73, 14.06, 20.46, etc., it follows that $R_1 = 7.73/S_1 = 14.06/S_2 = 20.46/S_3\ldots$, or, in other words, the radius of the first coordination sphere (the distance to the nearest neighboring atom) can be determined from the value of the wave vector, corresponding to any maximum of the scattering intensity curve. The radius of the first coordination sphere can be easily found from the experimental scattering curve using the Ehrenfest equation

$$2R_1\sin\theta = 1.23\lambda\,, \tag{19}$$

where λ is the wavelength of the radiation used, and θ is the diffraction angle.

The determination of the radial distribution function of atoms reduces to calculating the integral in the equation

$$4\pi R^2\rho(R) = 4\pi R^2\rho_0 + \frac{2R}{\pi}\int_0^\infty S\,i(S)\sin(SR)\,\mathrm{d}S\,, \tag{20}$$

where $i(S) = \left[I(S) - NF^2(S)\right]/NF^2(S)$ is the structure part of the coherent scattering intensity per atom, N is the number of atoms in a unit volume, $F(S)$ is the scattering amplitude, $\rho(R)$ is the number of atoms per unit volume at distance R,

ρ_0 is the mean number of atoms per unit volume, and the area under the first maximum determines the coordination number.

Diffraction experiments yield X-ray patterns, which are dependences of X-ray radiation intensity scattered by the sample at the scattering angle. The primary processing of X-ray patterns includes calculating the atomic factor; corrections for anomalous scattering, polarization, absorption, and incoherent scattering; calculating the structural factor; and (with the use of the data obtained) calculating different functions of the radial distribution of atoms, namely, total, $4\pi r^2\rho(r)$, relative, $g(r) = \rho(r)/\rho_0$, and difference, $4\pi r^2[\rho(r) - \rho_0]$. The analysis of atomic radial distribution functions provides only averaged characteristics and, in addition, is not free of a number of drawbacks. First, they include the appearance of so-called 'false' maxima, caused by the fact that in real experiments the integration is performed in a certain finite interval rather than from zero to infinity. Another very frequent error is the overestimation of the coordination number associated with both the nonideal symmetry of the first maximum and the insufficient accuracy of determining the background.

To get more complete information on the amorphous phase structure, the construction of partial functions of radial distribution is used. For a binary alloy A–B, this means constructing several functions for pairs of atoms AA, AB, BA, and BB, which requires performing several independent experiments, e.g., using different types of radiation (X-rays, neutrons, electrons).

The structural factor calculated from experimental scattering curves for a two-component alloy is expressed as

$$S(Q) = \frac{1}{\langle b\rangle^2}\left(c_\mathrm{A}^2 b_\mathrm{A}^2 S_\mathrm{AA}(Q) + 2c_\mathrm{A}c_\mathrm{B}b_\mathrm{A}b_\mathrm{B}S_\mathrm{AB}(Q) + c_\mathrm{B}^2 b_\mathrm{B}^2 S_\mathrm{BB}(Q)\right), \quad (21)$$

where b_A and b_B are the amplitudes of coherent scattering for atoms A and B, c_A and c_B are the atomic concentrations of the components A and B, $\langle b\rangle = c_\mathrm{A}b_\mathrm{A} + c_\mathrm{B}b_\mathrm{B}$, and $Q = 4\pi\sin\theta/\lambda$ (2θ is the scattering angle, λ is the wavelength). This function is a superposition of partial functions $S_\mathrm{AA}(Q)$, $S_\mathrm{AB}(Q)$, and $S_\mathrm{BB}(Q)$, corresponding to pair correlations of the components A–A, A–B, and B–B. It is clear that, to determine the partial structural factors, it is necessary to obtain a system of three equations with different values of b_A or b_B.

There are various ways to determine the total structural factor $S(Q)$, referred to as Faber–Ziman and Bhatia–Thornton formalisms. In the formalism proposed by Faber and Ziman for the case of neutron scattering [84], the total structural factor is defined as follows:

$$S(Q) = \frac{1}{\langle b\rangle^2}\left[\frac{\mathrm{d}\sigma}{\mathrm{d}\Omega} - \left(\langle b^2\rangle - \langle b\rangle^2\right)\right], \quad (22)$$

where $\mathrm{d}\sigma/\mathrm{d}\Omega$ is the differential cross section of the coherent scattering of neutrons, and $\langle b\rangle = \sum c_i b_i$ (c_i and b_i are the concentration and the amplitude of the coherent scattering of neutrons by atoms of the i-th sort, respectively). According to Faber and Ziman, the partial structural factors describe the correlations between different chemical elements of the alloy. The total structural factor $S(Q)$ of a binary alloy AB contains partial structural factors $S_{ij}(Q)$ and is described by Eqn (21). The weighting factors before $S_{ij}(Q)$ change upon varying b_i. Since b_i are different for different isotopes of one element, using the isotopic substitution, it is possible to change the weight factors so that different partial structural factors differently contribute to $S(Q)$. The function of radial distribution of atoms $G(r)$ is given by a Fourier transform of the structural factor $S(Q)$.

Another way to determine the partial structural functions was proposed by Bhatia and Thornton [85]. It allows describing both concentration-concentration (CC) and number density-concentration (NC) correlations between the atoms. The total structural factor according to Bhatia and Thornton is determined as

$$S^*(Q) = \frac{\mathrm{d}\sigma/\mathrm{d}\Omega}{\langle b^2\rangle}. \quad (23)$$

The separation of $S^*(Q)$ into three partial structural factors in the case of binary systems is performed using the formula

$$S^*(Q) = \frac{1}{\langle b\rangle^2}\left(\langle b\rangle S_\mathrm{NN}(Q) + 2\langle b\rangle(b_\mathrm{A} - b_\mathrm{B})S_\mathrm{NC}(Q) + (b_\mathrm{A} - b_\mathrm{B})^2 S_\mathrm{CC}(Q)\right). \quad (24)$$

The total and partial functions of radial distribution of atoms (FRDAs) are determined by a Fourier transform of the corresponding structural factors.

According to Faber and Ziman, the partial FRDAs describe the correlations between the atoms of individual chemical elements. In the case of the Bhatia–Thornton formalism, the function $G_\mathrm{NN}(r)$ describes the topological short-range order independently of the chemical type of the atom, and $G_\mathrm{CC}(r)$ is determined by scattering by fluctuations in the concentration of atoms with different scattering capabilities b. The peaks of $G_\mathrm{NN}(r)$ correspond to coordination spheres. The minima of $G_\mathrm{CC}(r)$ mean that, at the corresponding position, there is a different sort of atom than at $r = 0$; the maxima correspond to coordination spheres from atoms of the same sort as the atom at $r = 0$. In the case of a statistical distribution of atoms, $G_\mathrm{NC}(r) = 0$. Different functions of both formalisms are related through simple linear equations.

As was mentioned above, to construct the partial functions, it is necessary to perform several independent experiments. At present, the methods of constructing total and partial functions of radial distribution are not used very often, although it is worth mentioning Refs [86–89]. This paper is of particular interest, because its authors compared the results of studies using X-ray and synchrotron radiation with those of *ab initio* calculations by the method of molecular dynamics. This comparison revealed the presence of strong chemical ordering in the liquid and amorphous alloy $Zr_{55}Cu_{30}Ni_5Al_{10}$ with the formation of Zr–Cu, Zr–Al, and Zr–Zr pairs, and allowed estimating the stability of short-range and medium-range order in the alloy studied.

It should be noted that, in the absolute majority of cases, when analyzing the structure of metallic glasses, only the radius of the first coordination sphere is evaluated; its changes under exposures of different kinds determine the distortion of the diffuse maxima (additional shoulder, peak splitting, etc.). In combination with other methods of investigation, such an approach appears to be more productive. Most often, an X-ray structural analysis is combined with transmission and high-resolution electron microscopy.

In describing crystallization processes, it is usually assumed that the nucleation and growth of nanocrystals

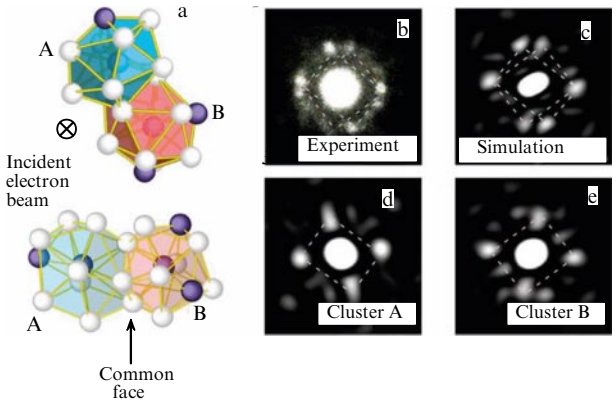

Figure 3. Beam diameter is 0.72 nm. (a) Two face-centered polyhedrons with a common axial orientation for Bragg diffraction. (b) Experimental patterns of nanoray diffraction. (c–e) Simulated patterns [90].

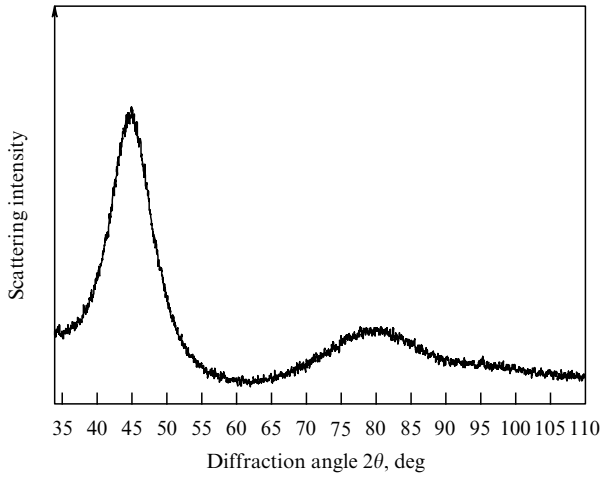

Figure 4. X-ray pattern of the $Al_{88}Ni_{10}Y_2$ amorphous alloy.

occur in a homogeneous amorphous phase. However, as already mentioned above, the amorphous structure can often be heterogeneous. The characteristics of the regions of heterogeneity and their origin, in turn, can differ substantially. In the amorphous phase, ordered regions can be observed, in which the short-range order applies to a few coordination spheres. Such ordered regions were observed experimentally using the methods of high-resolution electron microscopy, nanoray diffraction, etc. [90] (Fig. 3).

An amorphous structure can evolve under external exposures and change its characteristics, including the homogeneity. The formation of regions with different types of short-range order, i.e., actually several amorphous phases within one alloy, is possible. The amorphous phase structure can also considerably change under both heating and deformation; in this case, regions with different chemical compositions and/or short-range orders arise. As a rule, such a structure is formed with an increase in temperature. The authors of Ref. [91] present a number of examples of the formation of a heterogeneous amorphous structure (nanoglass). It is shown that the tendency to form a heterogeneous amorphous structure depends on the chemical composition (Pd–Au–Si [92], $(Zr_{0.667}Ni_{0.333})_{1-x}B_x$ [93], Cu–Ti, and Ni–Y [94]). Since the regions of different chemical composition are formed from an initially homogeneous structure, this process is controlled by the volume diffusion; with an increase in temperature (and acceleration of diffusion mass transfer), the process is facilitated. This formation of a heterogeneous structure upon temperature growth has been observed in a number of alloys (Pd–Au–Si [95], $Fe_{67}Co_{18}B_{14}Si_1$ [71], $Ni_{70}Mo_{10}P_{20}$ [35, 36], etc.). An increase in the degree of amorphous phase separation with an increase in the temperature or duration of thermal treatment has been detected in many systems ($Fe_{90}Zr_{10}$ [95–97], Fe–P–C, Fe–B, Pd–Au–Si [98], Al–Ni–(La, Gd, Y) [99]). An investigation of aluminum-based alloys [100] has shown that the formation of a heterogeneous amorphous structure can occur directly in the process of melt hardening. The authors of Ref. [100] have found that, upon a decrease in the cooling rate during melt hardening, it is possible to get a heterogeneous amorphous structure directly in the process of cooling. At a high cooling rate, the hardened amorphous alloy $Al_{82}Ni_{15}Y_3$ was homogeneous; in the case of cooling with a lower rate, the formation of a structure consisting of two amorphous phases differing in composition and type of short-range order was observed. Upon subsequent heating, these amorphous phases crystallized with the formation of different crystalline phases Al and Al_3Ni, the crystallization of two amorphous phases having begun not simultaneously.

Studies of phase separation processes in an amorphous structure are usually carried out using X-ray diffraction or transmission electron microscopy. A typical X-ray pattern of a homogeneous amorphous alloy is a scattering curve with an intense first diffuse peak and diffuse maxima sequentially decreasing in intensity (Fig. 4).

In the process of formation of a heterogeneous amorphous structure, regions differing in chemical composition and/or type of short-range order are formed in the sample. These regions are characterized by different minimal distances between atoms (or different radii of the first coordination sphere). In this case, the observed pattern of X-ray scattering is a superposition of scattering curves from each of the forming amorphous phases. In an experimental X-ray pattern, this manifests itself in a distortion of the shape of the maxima, the appearance of a shoulder, or even the splitting of the major peak into several peaks. Figures 5 and 6 show examples of such a change in X-ray patterns.

As was already noted, finding the distance between atoms (first coordination sphere radius) in an amorphous structure is implemented using X-ray scattering curves.

Studies using the transmission electron microscopy method also allow observing the appearance of inhomogeneity regions in an amorphous structure. Figure 7a presents an electron microscopy image of the $Al_{87}Ni_8La_5$ heterogeneous amorphous alloy, and Fig. 7b, the corresponding electron diffraction pattern. In Fig. 7a, one can clearly see brighter and darker areas corresponding to the regions of different absorption contrast caused by the difference between the chemical compositions of these regions. The electron diffraction pattern demonstrates two diffuse rings corresponding to two amorphous phases of different chemical composition with different radii of the first coordination sphere.

It should be noted that the formation of a heterogeneous structure is most actively developed at the initial stage of the treatment. This process has been thoroughly investigated by the example of the $Al_{87}Ni_8La_5$ amorphous alloy [101]. When studying this alloy, it was found that, in the X-ray pattern of

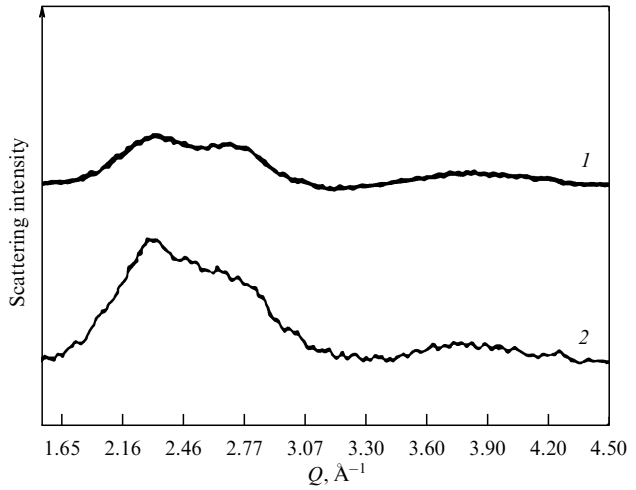

Figure 5. X-ray pattern of the $Pb_{60}Pd_{40}$ amorphous alloy [32] obtained with Cu K_α (*1*) and Mo K_α (*2*) emissions. *Q* is the wave vector.

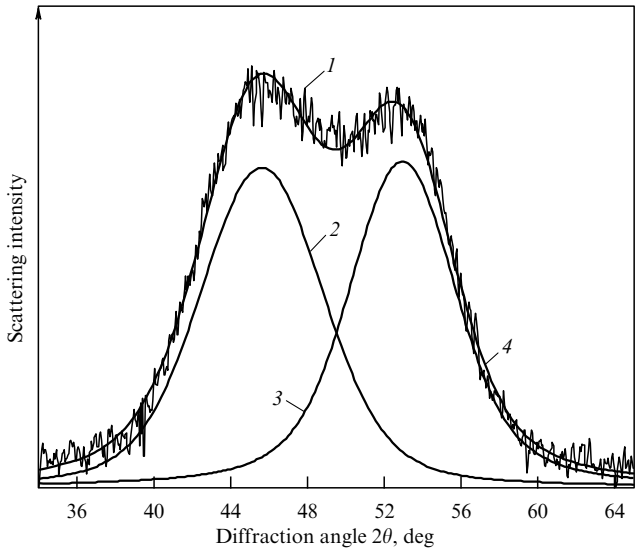

Figure 6. X-ray pattern of the $Al_{85}Ni_{12}Y_3$ amorphous alloy [100]. *1* — experimental curve, *2*, *3* — diffuse haloes corresponding to two amorphous phases, *4* — the sum (*2* + *3*) curve.

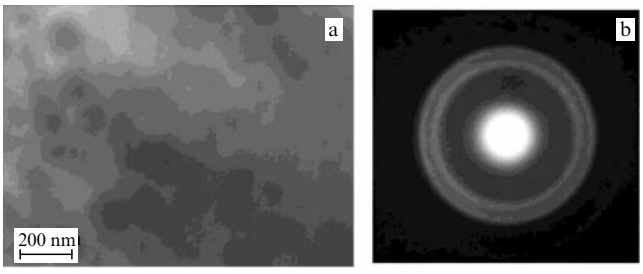

Figure 7. X-ray microscopy image (a) and electron diffraction pattern (b) of a heterogeneous amorphous structure.

amorphous samples immediately after hardening, the first diffuse maximum is symmetric, but in the course of hardening, it acquires a shoulder from the large-angle side, the degree of the maximum distortion growing with the increase in the annealing duration (Fig. 8). Figure 9 shows the difference in the angular position of diffuse maxima corresponding to two amorphous phases (curves *3* and *4* in Fig. 8) versus the

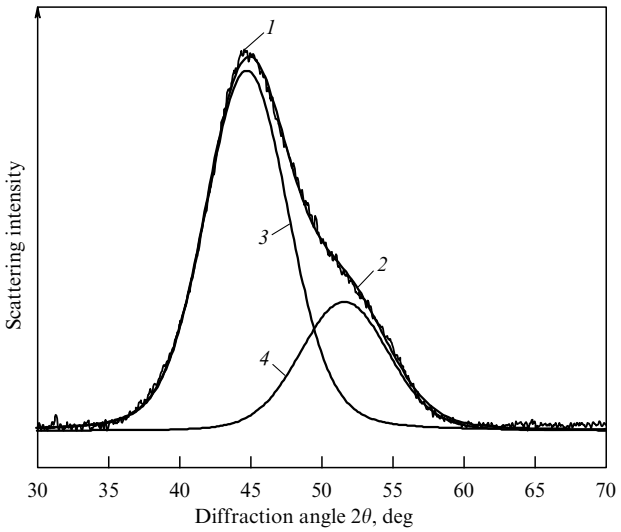

Figure 8. X-ray pattern of the $Al_{87}Ni_8La_5$ amorphous alloy after annealing at 150 °C for 25 hours [98]: *1* — experimental curve, *2* — summary envelope, *3*, *4* — reflections from two amorphous phases.

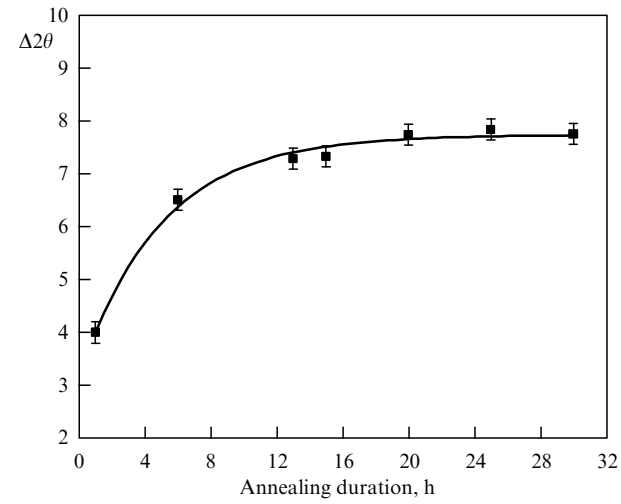

Figure 9. Difference between the positions of diffuse peaks versus annealing duration for the $Al_{87}Ni_8La_5$ amorphous alloy at 150 °C [101].

duration of the amorphous sample annealing. The increase in this difference with time reflects the separation of the diffuse maxima in the process of annealing, i.e., the growing difference in the first coordination sphere radii or interatomic distances in two new-forming amorphous phases. An analysis of atomic size and alloy composition shows that two diffuse maxima correspond to the regions enriched and depleted with lanthanum (and/or nickel). The left sub-peak corresponds to the amorphous phase with a greater radius of the first coordination sphere (Fig. 8, curve *3*); this amorphous phase is enriched with lanthanum (the larges atom in the alloy studied).

It is seen that, at the initial stage of annealing, the separation of the amorphous phase is more intense (the difference between the angular positions of the peaks noticeably grows), but, after some time (about 12 hours), the separation process finishes and no further change in the position of the maxima occurs.

The formation of a heterogeneous amorphous structure, naturally, leads to a change in the material properties, such

as thermal stability, Curie temperature [102], and plasticity [103, 104].

2.2.2 Formation of nanocrystals in a nanoglass. In the process of devitrification of a heterogeneous amorphous structure, the formation of crystals occurs independently in each sort of region. In this case, crystalline phases appear whose composition and short-range order correspond to the short-range order in the amorphous phase immediately before the beginning of crystallization. The formation of nanocrystals in a heterogeneous amorphous phase is studied mainly in alloys based on aluminum and nickel. What is the reason for choosing these materials? As shown above, the formation of a heterogeneous amorphous structure is most simply fixed using the methods of X-ray diffraction or transmission electron microscopy, although the second method is substantially more laborious. To make the distortion of a diffuse maximum in an X-ray or electron diffraction pattern noticeable, the differences among the first coordination sphere radii of regions with different chemical compositions and different types of short-range order should be large enough.

In many systems, it is extremely difficult to observe the separation. For example, the amorphous alloys of the Fe–B system also experience separation according to some data, so that amorphous phases with different concentrations of boron are expected to arise. However, because of the weak scattering capability of boron, it is difficult to detect this separation in X-ray patterns. In such alloys, the separation can be observed using the method of small-angle scattering of X-rays. This method allows detecting electron density inhomogeneities in the structure of the region; however, like any other method, it has its own limitations. In particular, to detect regions of electron density inhomogeneity, there should be many such regions, and the difference in electron density between these regions and the surrounding amorphous matrix should be substantial. Therefore, the formation of nanocrystals of the heterogeneous amorphous phase has been studied mainly in systems where the formation of a nanoglass was reliably established.

As a result of the experiments performed, it was shown that, for example, in the amorphous $Ni_{70}Mo_{10}B_{20}$ alloy [79], in the process of heterogeneous structure crystallization, nanocrystals of three phases are formed: fcc Ni, fcc solid solution of Mo in Ni, and the orthorhombic phase of Ni_3B. The crystallization of each phase occurs in its 'own' amorphous region. The size of the resulting crystals does not exceed 50 nm, which corresponds to the size of inhomogeneity regions in the heterogeneous amorphous structure before the beginning of crystallization. During the crystallization of a homogeneous amorphous alloy with the same composition, the formation of eutectic $Ni + Ni_3B$ colonies of substantially larger sizes occurs. Crystallization occurred in a similar way in the amorphous $Ni_{70}Mo_{10}P_{20}$ alloy [35]: the devitrification of a homogeneous amorphous structure gave rise of the formation of eutectic colonies consisting of relatively large crystals of Ni and Ni_3P. On the contrary, in the case of crystalizing a heterogeneous amorphous structure, the grain structure arose, and the formation of Ni and Ni_3P phases did not occur simultaneously; however, each of the phases formed in its 'own' concentration region. In amorphous alloys of the Al–Ni–*RE* (*RE* = La, Gd, Y) system [12, 21], additional separation of the amorphous matrix was observed in the process of crystallization. In some cases, the separation of the amorphous phase with subsequent crystallization can occur through the mechanism of spinodal decomposition (see Section 2.3 below). Below, we will compare at length structures formed from the homogeneous and heterogeneous amorphous phases.

2.3 Formation of nanocrystals through spinodal decomposition

Amorphous alloy crystallization through the spinodal decomposition mechanism is rather rare [36, 92, 94]. One of the first studies in which the possibility of spinodal decomposition was noted was devoted to the Rd–Au–Si system [89]. Crystallization of amorphous alloys of this system strongly depended on the concentration of components, and in the $Pd_{0.74}Au_{0.08}Si_{0.18}$ composition, the authors of Ref. [92] observed spinodal decomposition. The structure change during the spinodal decomposition has been most thoroughly investigated in the Fe–Zr system [36], where it was shown that long-time low-temperature annealing gives rise to a chain of transformations: homogeneous amorphous phase → heterogeneous amorphous phase → two solid solutions of Zr in α-Fe of different concentrations → equilibrium α-Fe + Fe_3Zr phases. All stages of the transformation took place in regions that did not change in size; in the course of the structure transformation, a gradual formation of sharper boundaries between particles was observed. The size of nanocrystals in the crystallized structure was 10–30 nm.

3. Possibility of amorphous structure rejuvenation

Amorphous metallic alloys possess good properties [105–108], which can be noticeably improved by low-temperature annealing (e.g., annealing in a magnetic field), etc. However, in this case, and even during mere aging, embrittlement occurs, which limits the potentialities of their practical application. The main cause of embrittlement is an increase in the short-range order degree, which leads to the formation of regions with different local structures and, naturally, properties. In parallel, the free volume concentration decreases (increasing the density within 0.5%), leading to a decrease in the atomic mobility (the structure becomes denser and more ordered).

Based on general considerations, to restore the plasticity, one should increase the free volume concentration in the amorphous alloy and reduce the degree of its 'crystallicity'. One of the first attempts to restore the plasticity of iron-based alloys ($Fe_{40}Ni_{40}B_{20}$, $Fe_{40}Ni_{40}P_{14}B_6$) was associated with exposing samples to thermal neutrons [109–113]. The above papers describe experiments, in particular, on increasing the plasticity of the $Fe_{40}Ni_{40}P_{14}B_6$ alloy. Exposing boron-containing alloys to thermal neutrons induces the ^{10}B (n, α) Li reaction with the formation of high-energy fission fragments that cause a high-power 'self-irradiation' of the material and destruction of ordered regions in the amorphous phase. As a result, the plasticity of the amorphous alloy increases. It should be said that the irradiation effect on the plastic properties of amorphous materials is controversial, and a decrease in plasticity has been observed in a number of papers. This is probably due to a number of processes that take place under the irradiation: breaking the clusters and their easier restoration (since the structure imperfection is increased), an increase in temperature leading to a decrease in the free volume concentration, etc. The dominance of one

factor or another will exert the decisive effect on the change in mechanical properties.

Another way to restore the plasticity was to use a plastic deformation [114–116] leading to noticeable atomic restructuring. The authors of Ref. [116] hypothesized that the structural changes under deformation can be a result of local heating induced by the deformation. In recent years, a new and more efficient method of structure restoration, the method of cryogenic thermocycling, has been under development, which consists of thermocycling within a temperature interval between the temperature of liquid nitrogen and room temperature or higher [117–119]. This process was called rejuvenation. The idea of the new method is based on the assumption of a structural change under mechanical stress, induced by a nonuniform change in the thermal expansion coefficient. If a structure is inhomogeneous (nanoglass being a typical example), then there are regions in it differing in chemical composition, density, and other properties, and characterized by different coefficients of thermal expansion as well. A sharp temperature change in such a structure will induce stresses leading to local atomic restructuring [118, 119]. This method was first applied to the $Zr_{55}Cu_{30}Al_{10}Ni_5$ alloy [118]; however, no visible changes in the structure were detected. Later, it appeared possible to observe structural changes in the $Zr_{46}Cu_{38}Al_8Ag_8$ inhomogeneous amorphous alloy [120], as well as to completely restore the amorphous phase in the partially crystalline $Al_{88}Ni_6Y_6$ and $Al_{87}Ni_8Gd_5$ alloys [121, 122]. In the latter case, the difference between thermal expansion coefficients increased at the expense of the formation of a small number of nanocrystals in the amorphous phase followed by the cryogenic thermocycling of the structure, consisting of the amorphous phase and aluminum nanocrystals uniformly distributed in it.

Figure 10 shows the initial segment of the X-ray pattern of the $Al_{88}Ni_6Y_6$ alloy before the beginning of cryogenic thermocycling, and Fig. 11 shows the electron diffraction pattern of the structure. It is seen that in the alloy there is a small number of nanocrystals (in the X-ray pattern, a blackened peak corresponds to them). After performing the cryogenic thermocycling, the intensity of reflection from the nanocrystals (Fig. 12) considerably lowered, and the number of nanocrystals in the electron diffraction image (Fig. 13) decreased greatly. These results directly indicate the rejuvenation of the amorphous structure in the process of cryogenic thermocycling. With an increase in the treatment duration, the amorphous structure was completely rejuvenated. The rejuvenation of the amorphous structure has naturally led to the restoration of the material plasticity.

How can the rejuvenation of an amorphous structure occur? As already mentioned above, in a heterogeneous amorphous structure, there are regions differing in chemical composition and, therefore, characterized by different thermal expansion coefficients. A sharp change in temperature in such a structure facilitates the appearance of stresses, leading to local atomic restructuring. The magnitude of arising thermally induced stresses can be determined by the formula [123]

$$\sigma_p = \frac{\Delta\alpha\,\Delta T}{(1+\nu_m)/2E_m + (1-2\nu_p)/2E_p}\,, \qquad (25)$$

where σ_p is the mean stress inside the particles, $\Delta\alpha$ is the difference between the thermal expansion coefficients of the particles and the matrix, ν_m and ν_p are the Poisson coefficients for the matrix and the particles, and E_m and E_p are the Young moduli for the matrix and the particles, respectively.

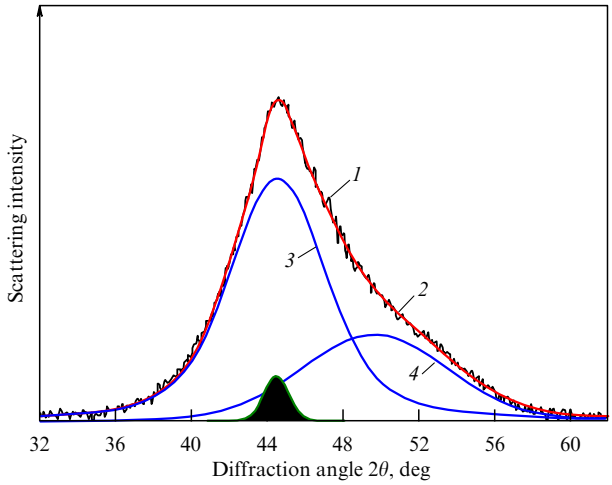

Figure 10. X-ray pattern of the $Al_{88}Ni_6Y_6$ alloy before the beginning of cryogenic thermocycling [122]: *1* — experimental curve, *2* — summary envelope, *3*, *4* — reflections from two amorphous phases.

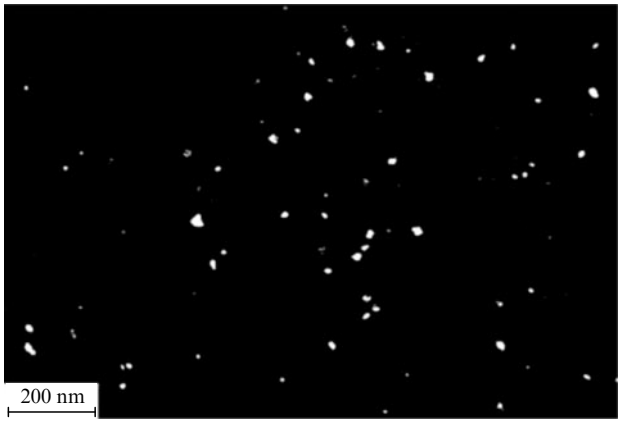

Figure 11. Transmission electron microscopy image of the $Al_{88}Ni_6Y_6$ alloy before the beginning of cryogenic thermocycling [122].

The mean stress σ_m in the matrix is determined from the equation

$$f\sigma_p + (1-f)\sigma_m = 0\,. \qquad (26)$$

Formula (25) works when the volume fraction of the second-phase particles does not exceed 10%. The general formula with the fraction of particles f taken into account has the form [123]

$$\sigma_p = \frac{\Delta\alpha\,\Delta T}{1/3K_p + 1/4(1-f)\,G_m + f/3(1-f)K_m}\,, \qquad (27)$$

where K_p, K_m are the bulk moduli of the particles and the matrix, respectively, and G_m is the shear modulus of the matrix.

From Eqns (26) and (27), it follows that the stresses within the particles and in the matrix have opposite signs. This means that if there is a tensile stress in the particles, then in the matrix the stress is compressive and vice versa. The absolute value of the stress within particles decreases according to an approximately linear law with an increase in their proportion, whereas the stress in the matrix increases. Estimates in [121] have shown that, in the case of the $Al_{87}Ni_8Gd_5$ alloy, the stress inside Al nanocrystals can reach

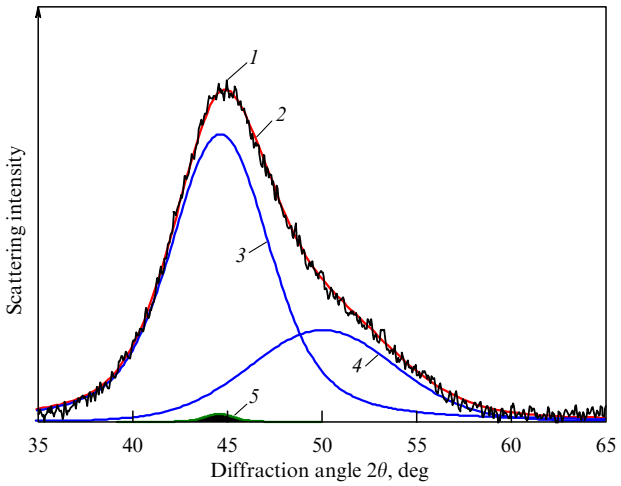

Figure 12. X-ray pattern of the $Al_{88}Ni_6Y_6$ alloy after cryogenic thermocycling [122]: *1* — experimental curve, *2* — summary envelope, *3*, *4* — reflections from two amorphous phases.

Figure 13. Transmission electron microscopy image of the $Al_{88}Ni_6Y_6$ alloy after cryogenic thermocycling [122].

90 MPa in the temperature interval of 77–393 K. Comparing the obtained values with the stress of dislocation generation and taking into account the thermocycling duration allowed the authors of Ref. [121] to conclude that the stresses arising under cryogenic thermocycling can cause deformational amorphization.

4. Formation of a heterogeneous structure and nanocrystals under deformation

Plastic deformation of amorphous alloys at low temperatures is known to be highly localized and, in fact, is implemented in narrow zones — the shear bands, leaving the main part of the amorphous phase virtually unaffected. The structure in the shear bands differs from that in the rest of the amorphous phase. The investigations carried out have shown that in the shear bands the diffusion coefficient at room temperature is five-six orders of magnitude higher than in the surrounding amorphous matrix [124]. The reasons for the increase in the diffusion coefficient by a few orders of magnitude can be diverse. Usually, the increase in the diffusion coefficient in the shear bands is associated either with a local great but short-duration (about 30 ps) increase in temperature in this region [125–127] or with an increase in the free volume fraction (with a decrease in density) in the shear band [16, 128, 129]. It is important that, as a result of deformation, two structural components arise: the amorphous regions separated from each other by visible interfaces and the interfaces themselves (the regions containing an increased free volume). Such boundary regions also have an amorphous structure, but possess lower density.

Many papers, among which the review by Greer et al. [130] should be distinguished, are devoted to the structure of shear bands in amorphous alloys as such. In this review, the issues of nucleation, structure, and propagation of shear bands are considered in detail. However, many issues related to the formation of such an unusual structure and the structure of boundary regions themselves remain open and continue to be widely studied at present. In particular, a group of Russian researchers [131] hypothesized that, under certain deformation regimes, systems of shear bands form in a material, and it is exactly these systems of bands that separate amorphous regions, forming a kind of nanoglass. Such specific structures with a high density of nanosized shear bands, analogous to the structure of a nanoglass, have been observed by the authors in various systems of amorphous alloys based on Zr, Au, and Ti after twisting under high pressure, in particular, in the alloys of the Ti–Ni–Cu system [132]. It was found that the structure that forms consists of nanosized amorphous clusters separated by amorphous boundaries, the structure depending on the temperature at which the deformation is carried out [133, 134]. The authors of these papers have established that the boundary region is a shear band, which, in turn, is formed by a group of closely spaced bands separated from each other by 10–20 nm.

Under great deformation, the structure of the bands can be rather branched. There are studies demonstrating that the treatment of an amorphous material under high degrees of deformation makes it possible to obtain a material with a fairly high density of shear bands, which largely change the local structure of the material [135, 136]. Naturally, such a structure cannot but affect the process of amorphous phase crystallization. Studies of deformation processes and nanocrystalline structure formed in the course of deformation are being carried out with a variety of alloys, including comparative studies of nanocrystal formation under heating and deformation [137].

In addition to the formation of shear bands, deformations can also give rise to an anisotropic amorphous structure [138] and a heterogeneous amorphous structure of the same type as that produced by thermal treatment. Figure 14 presents an X-ray pattern of the $Al_{88}Ni_6Y_6$ alloy after pressure treatment at $P = 5$ GPa [139]. The reflections marked with crosses correspond to BN (boron nitride powder served as a pressure-transmitting medium). The diffuse maximum is seen to be asymmetric, which testifies to the formation of a heterogeneous amorphous structure.

Amorphous phase separation and the formation of a heterogeneous amorphous structure can occur in the process of rolling, too. Figure 15 shows part of an X-ray diffraction pattern (the region of the first diffuse maximum) of the amorphous $Al_{88}Ni_{10}Y_2$ alloy deformed by the method of multiple rolling [140].

In this case, in addition to the heterogeneous amorphous phase (diffuse maxima *5* and *6*), a small number of aluminum nanocrystals is formed (peaks *3* and *4* are (111) and (200) reflections from the Al nanocrystals). The X-ray patterns (see Figs 14, 15) testify to the fact that, under deformation in

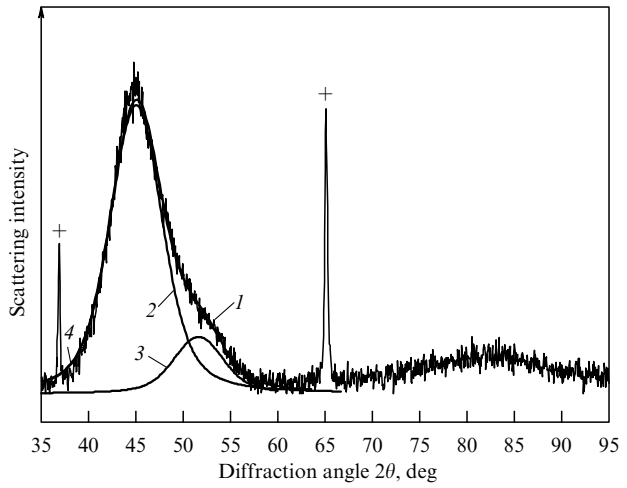

Figure 14. X-ray pattern of the $Al_{88}Ni_6Y_6$ alloy after pressure treatment at $P = 5$ GPa: *1* — experimental curve, *2*, *3* — reflections from two amorphous phases, *4* — summary envelope.

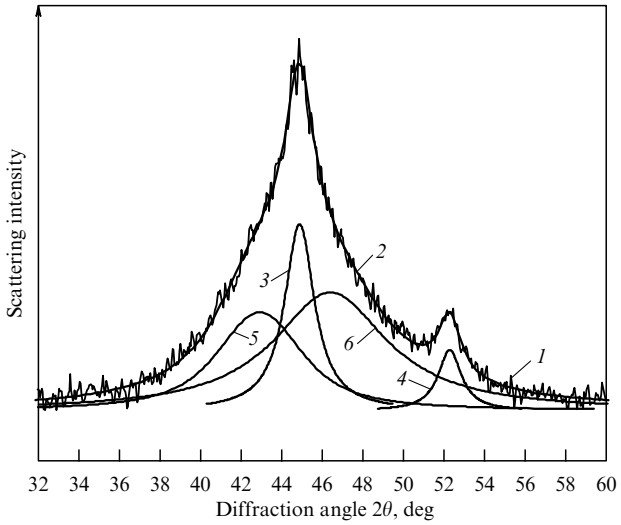

Figure 15. Segment of an X-ray pattern corresponding to the region of the first diffuse halo: *1* — experimental curve, *2* — summary envelope, *3*, *4* — reflections from aluminum nanocrystals, *5*, *6* — reflections from the amorphous phase.

$Al_{88}Ni_6Y_6$ and $Al_{88}Ni_{10}Y_2$ amorphous alloys, the formation of a heterogeneous amorphous structure occurs. Naturally, the deformation of the amorphous phase causes a change in the material properties [141].

An important feature of deformation-induced nanocrystallization is the significant extension of the group of materials in which the formation of nanostructures is possible. To create a nanostructure from an amorphous alloy, the method of intense plastic deformation, namely, twisting under high pressure, is most frequently used. In the abovementioned amorphous Fe–Si–B alloy, no nanocrystals are formed during the thermal treatment because of the high diffusion coefficient of boron and, therefore, rapid growth of the crystals. By means of intense plastic deformation in amorphous Fe–Si–B and Fe–B alloys, a nanostructure has been formed, which allowed obtaining new materials with good magnetic properties. It was shown in [142] that, upon achieving a certain level of deformation, nanocrystallization occurs in an amorphous alloy. Prolonged zones (Fig. 16) in which nanocrystals can have a preferable orientation can

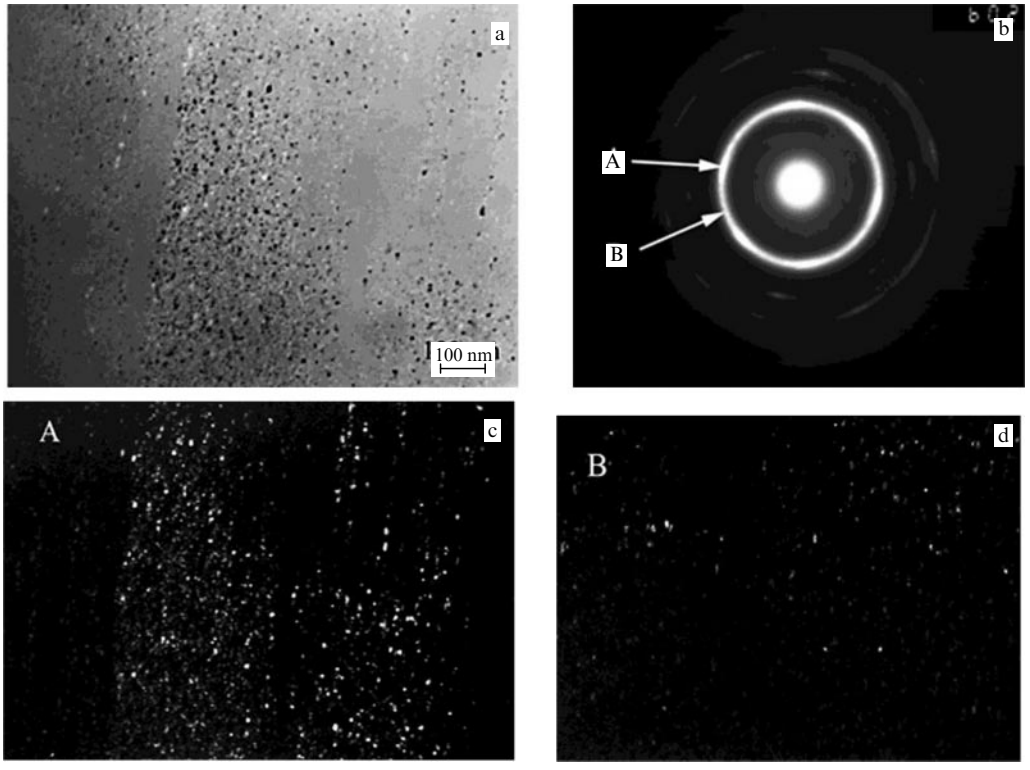

Figure 16. Structure of the $Fe_{78}Si_{13}B_9$ alloy deformed by twisting under a pressure of 4 GPa [142]: (a) bright-field electron microscopic image, (b) electron diffraction pattern, and (c, d) dark-field electron microscopy image of segments A and B of the ring, marked with arrows in the electron diffraction patterns.

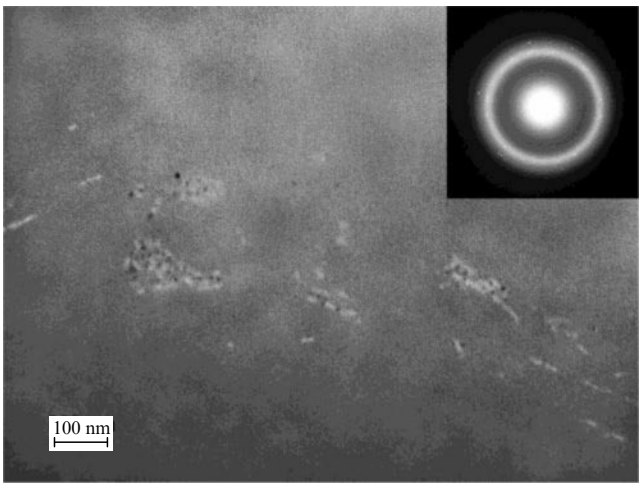

Figure 17. Structure of the $Al_{85.1}Ni_6Co_2Gd_6Si_{0.9}$ alloy after rolling and aging at room temperature for a few months [144].

arise in the samples, which is confirmed by the presence of high-intensity spots (one of them marked by the arrow A) on the ring in the electron diffraction pattern. Figure 16 presents a bright-field electron microscopy image of the structure of the deformed $Fe_{78}Si_{13}B_9$ alloy (a), the electron diffraction pattern (b), and the dark-field electron microscopy images (c, d) of the ring segments A and B, marked with arrows in the electron diffraction pattern. The dark-field image of the structure in the higher-intensity part of the ring is seen to contain a large number of nanocrystals (prolonged zone), whereas in the dark-field image corresponding to the lower-intensity part of the ring (B), there are many fewer nanocrystals, and they are placed randomly.

The mean size of nanocrystals in this sample is 6 nm. The proportion of the nanocrystalline phase becomes greater with increasing deformation degree and reaches the value of $\sim 50\%$; the size of the nanocrystals remains unchanged. The formation of nanocrystals leads to a substantial increase in the saturation magnetization (by nearly 40%) without a noticeable change in the coercive force.

The formation of nanocrystals in the process of intense plastic deformation occurs mainly in the shear bands and their neighborhood [17]. As noted above, the shear bands have a looser structure and the values of the diffusion coefficient in them is significantly higher than in the surrounding amorphous matrix [2, 17, 120, 143]. The increasing diffusion coefficient in the shear bands makes possible the formation of nanocrystals in them even at room temperature [2, 17, 143, 144]. Thus, for example, the predominant formation of nanocrystals in the shear bands in the $Al_{88}Y_7Fe_5$ alloy has been observed after termination of a tensile deformation [17]. Similar results were obtained in aluminum-based alloys ($Al_{85.1}Ni_6Co_2Gd_6Si_{0.9}$) deformed by rolling [144]. After the end of deformation and aging at room temperature for a few months, the shear bands appeared to be filled with nanocrystals, whereas in the main amorphous matrix, the number of nanocrystals was insignificant (Fig. 17).

An intense plastic deformation can lead not simply to nanocrystal formation, but to additional refinement of crystals already formed. This phenomenon was observed in the nanocrystallization of amorphous alloys of Fe–B systems under the action of intense plastic deformation

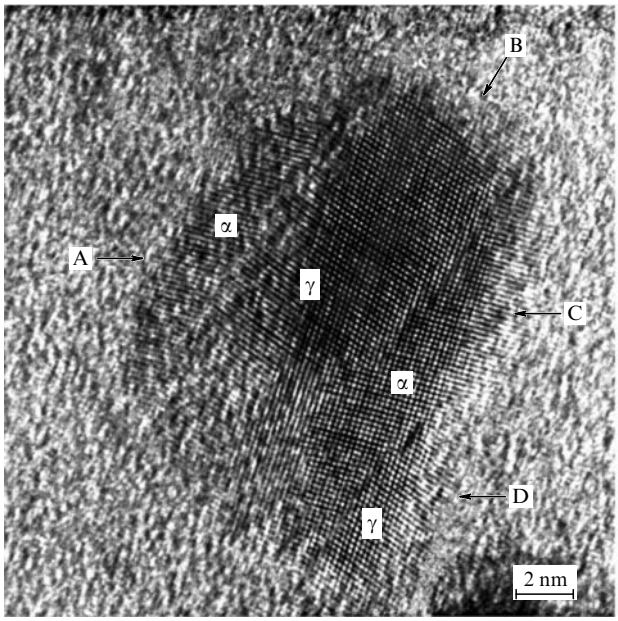

Figure 18. High-resolution electron microscopy image of the deformed $Fe_{80}B_{20}$ amorphous alloy [145].

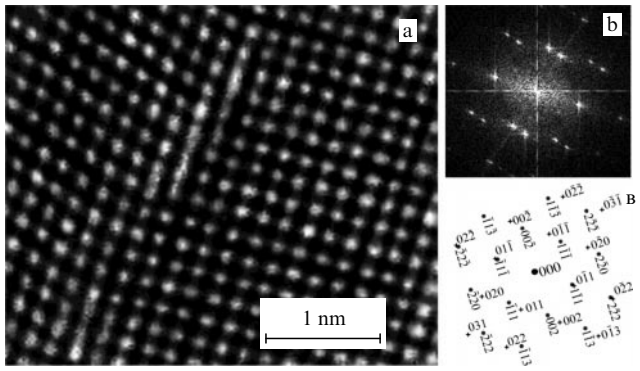

Figure 19. (a) High-resolution electron microscopy image of a nanocrystal, (b) electron diffraction pattern, (c) schematic diagram of electron diffraction pattern [145].

[145]. Upon twisting deformation of the amorphous $Fe_{80}B_{20}$ alloy under a pressure of 5 GPa at a temperature of 200 °C, the formation of α-Fe nanocrystals was observed. The mean size of the nanocrystals did not exceed 10 nm; however, individual nanocrystals about 20 nm in size were also present. The structure of these nanocrystals was layered and consisted of α-Fe and γ-Fe regions (Fig. 18). In this figure, the α regions have a bcc lattice (α-Fe, regions A and C), and the γ regions have an fcc lattice (γ-Fe, regions B and D).

A detailed analysis of the structure has shown that the lattices of the regions with the α-Fe and γ-Fe structure are in certain orientation relationships that testify to a martensitic type of transformation. Figure 19 shows a high-resolution electron microscopic image of a nanocrystal (a), an electron diffraction pattern (b), and a schematic diagram of the electron diffraction pattern (c). The orientation relations were the Nishiyama–Wassermann relations, characteristic of a martensitic transformation; it was found that in larger nanocrystals an inverse martensitic transformation took place. Thus, the martensitic transformation can cause a

decrease in nanocrystal size (fragmentation of larger nanocrystals of α-Fe).

5. Structure and properties of nanomaterials produced in the course of thermal treatment and deformation

In a number of systems, the formation of nanocrystals in the amorphous phase can be implemented by both thermal treatment and deformation; however, the parameters of nanostructures greatly depend on the conditions of the external actions. Studies have shown that the nanocrystals formed in the process of deformation are usually more disperse than nanocrystals produced by thermal treatment. However, the causes of this phenomenon are still not quite clear. Comparative studies allow clarifying how these structures can be formed under such different actions and how the material properties can change depending on the nanostructure parameters.

Many nanocrystalline alloys are known to be very strong [146–152]. For such materials, one of the most important issues is the interaction of nanocrystals with the shear bands in the process of deformation, in particular, it is important whether the nanocrystals can be an obstacle to the motion of the shear bands. Since the deformation of amorphous alloys occurs through the nucleation of propagation of shear bands, the size ratio of nanocrystals and shear bands is of primary importance, which can determine various mechanisms of their interaction [148, 153–156]. Deformation treatment by rolling is known to produce a large number of shear bands, which hamper the propagation of new deformation-induced shear bands [155, 156]. In turn, nanocrystals, depending on their chemical composition and size, can be virtually perfect or contain numerous linear defects, namely, defects of packing and dislocations [12, 157] that are carriers of deformation. Thus, for instance, in Ref. [12], it was shown that the presence of defects in nanocrystals depends on both the dimension factor and the uniformity of distribution of the components. When the nanocrystals are solid solutions, the probability of defect formation increases, and the size at which the defects can form substantially decreases.

The formation of a structure with a large number of intersecting shear bands noticeably affects the plasticity and mechanical characteristics of the material. In recent papers, it was shown that, in an alloy of the Zr–Cu–Al–Fe system, a deformation with the appearance of a large number of inhomogeneities in the form of shear bands in the amorphous matrix decreases the elasticity modulus and hardness and increases the sensitivity to the deformation rate compared to the initial material [158–160]. It was found that, upon the formation of nanocrystals in aluminum-based amorphous alloys, the microhardness increases [161], the dependence of microhardness on the nanocrystal size not corresponding to the Hall–Petch law.

As is known, the dependence of microhardness (and strength) of a material on grain size (the Hall–Petch dependence [162, 163]) is one of the important laws of physical materials science. According to this dependence, the yield stress σ_τ is inversely proportional to the square root of the grain diameter d:

$$\sigma_\tau = \sigma_0 + \frac{K_y}{d^{1/2}}, \quad H_V = H_{V0} + \frac{K_y}{d^{1/2}}, \tag{28}$$

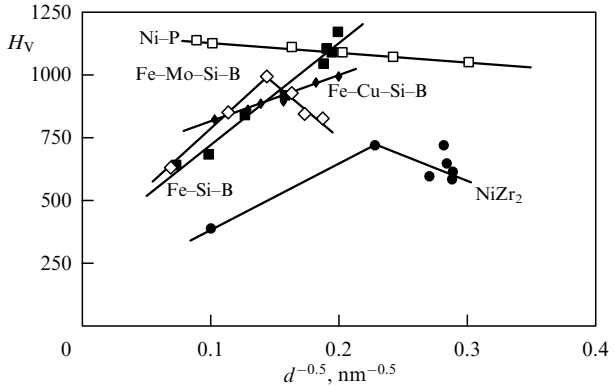

Figure 20. Dependence of microhardness of nanocrystalline alloys on the size of nanocrystals [164].

where σ_0 is the lattice friction stress arising in the motion of a single dislocation, independent of the grain size, K_y is a (positive) constant, depending on the resistance of grains to the motion of dislocations, and H_V is the Vickers microhardness, $\sigma_\tau \approx H_V/3$. However, in the case of nanocrystalline materials with a grain size less than 50 nm, this dependence is violated. Figure 20 shows the microhardness dependence of nanocrystalline alloys on the size of the nanocrystals [164].

The authors of Refs [164, 165] have established the presence of a certain critical grain size. If the grain size in a material is greater than the critical one, the Hall–Petch law is valid; if it is smaller, deviations from this law or even an inverse dependence are observed. Obviously, direct application of the Hall–Petch law to nanocrystalline materials is impossible. In principle, the Hall–Petch equation is applicable to the strengthening caused by the accumulation of dislocations on such an obstacle as grain boundaries. It was already mentioned above that the structure of nanocrystalline materials consists of nanocrystals separated from each other by regions of the amorphous phase. Nanocrystals are distributed in an amorphous matrix, their size being comparable to the thickness of the amorphous phase between them. In the analysis of nanocrystalline materials, an analogy is often drawn between a change in nanocrystal size and hardening according to the Hall–Petch equation. Thus, for example, in nanocrystalline materials, the critical grain size was also observed, beginning from which the dependence on the grain size becomes inverse to the Hall–Petch relation. As a rule, in amorphous nanocrystalline alloys after the end of primary crystallization, an anomalous behavior of the Hall–Petch relation is observed.

Figure 21 presents X-ray patterns of the $Al_{88}Ni_2Y_{10}$ alloy in the initial amorphous state (curve *1*) and after the end of the first stage of crystallization (curve *2*). The microhardness of the initial homogeneous amorphous alloy was 270 MPa. After the end of the first stage of crystallization, the sample is two-phase and contains aluminum nanocrystals and an amorphous phase of modified composition, left after the extraction of the nanocrystals. The microhardness of such a sample appears to be much higher and amounts to 440 MPa.

Thus, during the formation of nanocrystals, the microhardness (and strength) of alloys increases. However, in the process of further transformation of the structure with the decay of the residual amorphous phase and the formation of intermetallides, the microhardness decreases. Figure 22

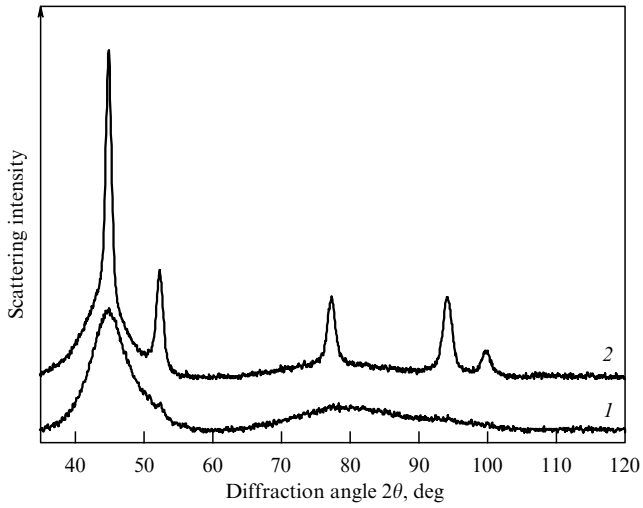

Figure 21. X-ray patterns of the $Al_{88}Ni_2Y_{10}$ alloy in the initial amorphous state (*1*) and after the end of the first stage of crystallization (*2*).

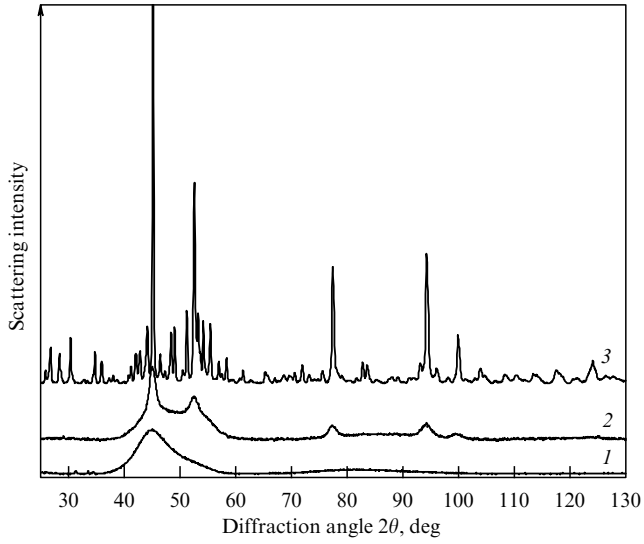

Figure 22. X-ray patterns of the $Al_{88}Ni_6Y_6$ alloy: heterogeneous amorphous phase (*1*), structure after the end of the first stage of crystallization (*2*), and equilibrium crystalline structure (*3*).

shows X-ray patterns of the $Al_{88}Ni_6Y_6$ alloy after the deformation not leading to crystallization (heterogeneous amorphous phase, curve *1*), after the end of the first stage of crystallization (curve *2*), and after the formation of an equilibrium crystalline structure (curve *3*). The microhardness of the samples in this case is 260, 420, and 300 MPa, respectively. Note that the composite amorphous-nanocrystalline structure has the maximal microhardness (and, correspondingly, strength).

It is clear that the properties of nanocrystalline materials depend not only on the size of nanocrystals but also on other structural parameters: the phase composition, nanocrystalline phase proportion, morphology of nanocrystals, etc. The changes in the structure greatly affect the magnetic properties of the material, too. Figure 23 shows the change in the coercive force under the thermal treatment of metallic glasses $Fe_{75}Si_{11}B_{10}Nb_3Sn_1$, $Fe_{76}Si_{11}B_{10}Nb_3$, and $Fe_{78}Si_{11}B_{10}Sn_1$ [166]. It is seen that, with the structural change in the process of annealing, the magnetic properties vary in a substantially

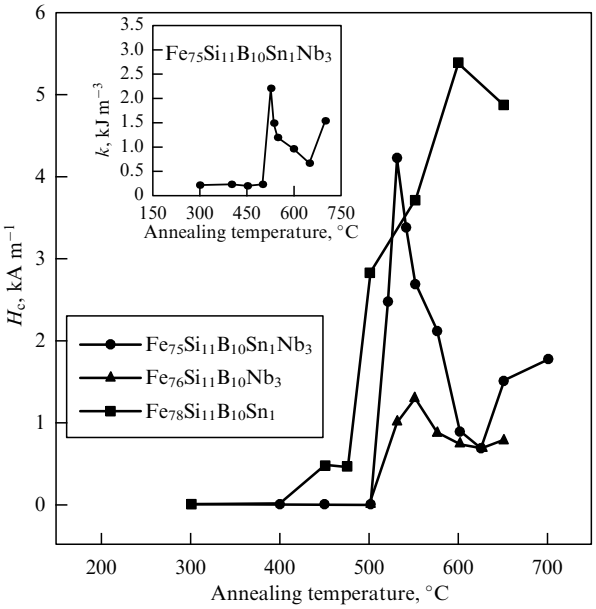

Figure 23. Variation in coercive force H_c with annealing temperature [166]. Inset: dependence of anisotropy on annealing temperature.

nonmonotonic way, and the degree of the properties changes, depending of the alloy composition.

Alloys with a combined amorphous-nanocrystalline structure possess very high magnetic properties. One of the examples is Finemet ($Fe_{74}Si_{13}B_9Cu_1Nb_3$) [50, 167]. Finemet-type alloys possess a perfect collection of hysteresis properties. Thus, the initial permeability and coercive force can be 1,000,000 and 0.5 A m^{-1}, respectively. Other iron-based alloys — Fe–*M*–B (*M* = Zr, Hf, Nb) [168] — have values of saturation induction above 1.5 T, i.e., close to the values of saturation induction of high-silicon electrotechnical steels, and an effective permeability above 30,000 at 1 kHz [169]. The nanocrystalline structure consists of α-Fe crystals 10–20 nm in size in all alloys of this group. The structure and properties of Finemet-type allows are being studied very widely [167, 170–179]. A significant number of these studies relate to the investigation of the $Fe_{74}Si_{13}B_9Cu_1Nb_3$ alloy, but there are many compositions doped with other components [180–190]. All these alloys have perfect soft magnetic hysteresis properties (low coercive force and high permeability).

The necessary conditions for achieving perfect soft magnetic properties are a small energy of magnetocrystalline anisotropy and very low saturation magnetostriction ('zeroing' the magnetoelastic anisotropies). What makes it possible to realize such conditions in amorphous-nanocrystalline alloys? There are several factors. A decrease in the anisotropy leads to an improvement in soft magnetic properties. The alloys are two-phase and consist of an amorphous matrix and nanocrystals of solid solution of silicon in bcc iron Fe(Si) with a size of about 10 nm. Both the coercive force and the permeability are known to depend on the anisotropy, which, in turn, consists of the magnetocrystalline, magnetoelastic, and induced anisotropy contributions. In an amorphous alloy, the magnetocrystalline anisotropy is absent. The model that determines the anisotropy and the corresponding coercive force depending on the crystal size belongs to G Herzer [191]. According to this theory, in a domain of a nanocrystalline alloy, there are many randomly oriented nanocrystals. As a result, within each domain, the averaging

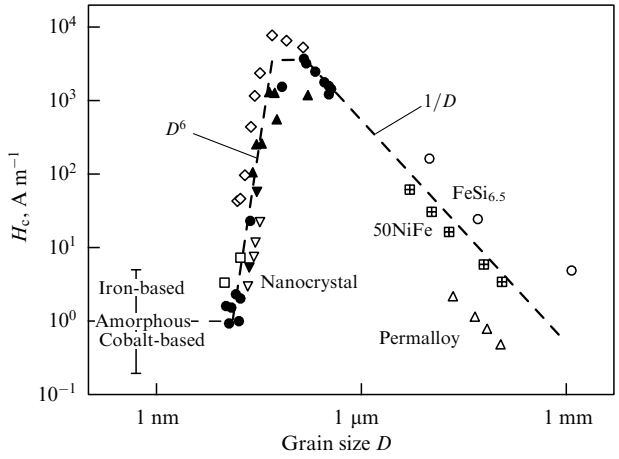

Figure 24. Dependence of the coercive force on grain size for soft magnetic alloys [191].

of the directions of easy magnetization axes occurs, and the total magnetocrystalline anisotropy becomes zero. According to this model, the coercive force is proportional to d^6, where d is the nanocrystal diameter. It so happens that, in these alloys, the amorphous matrix possesses positive magnetostriction and negative forming nanocrystals, so that at the nanocrystalline phase fraction of 70–80% their mutual compensation occurs. Therefore, the magnetoelastic part of the effective anisotropy, like the magnetocrystalline one, takes a value close to zero. The low effective anisotropy gives rise to unique soft magnetic properties of this group of alloys.

Figure 24 presents the dependence of the coercive force of the alloys on the grain size, which has already become classical. The black dots correspond to the Finemet alloy. The dependence is seen to have a substantially nonmonotonic character, and the coercive force changes dramatically with crystal size [191].

From the presented analysis, it follows that, to create materials with the required mechanical or magnetic properties, it is necessary to study the interrelation among the kind and parameters of external actions, nanostructure characteristics, and material properties.

6. Comparing the structures of nanomaterials formed under thermal treatment and deformation

As already mentioned above, nanocrystals obtained by deformation are usually smaller than those formed by thermal treatment [192]. In the course of investigations, it was also found that the crystallization process depends on the conditions of the amorphous phase preparation [193], and the nanostructure parameters can substantially depend on whether the process of nanocrystallization occurred in the homogeneous or heterogeneous phase [147, 194]. In particular, it was discovered that thermal treatment in various temperature intervals leads not only to a change in the amorphous phase structure but also to the formation of a crystalline structure with a substantially different crystal size under subsequent heating. Smaller crystals were observed when the crystallization was preceded by the formation of an inhomogeneous amorphous structure.

What could be the reason for the difference between nanostructures formed in a homogeneous or heterogeneous amorphous phase? An important specific feature of amorphous phase crystallization is the formation of those crystalline phases at the initial stage, in which the short-range order corresponds to the short-range order of these ordered regions. This means that the structural state of the amorphous phase before the beginning of crystallization should affect the structure resulting from the crystallization. As was mentioned above, a heterogeneous structure can arise due to both thermal treatment and deformation.

Investigations of nanocrystal formation under heating and deformation have been carried out on a large number of alloys [20, 142, 195–198]. In Refs [21, 22, 192], it was found that the formation of a heterogeneous amorphous structure in aluminum-based alloys accelerates the crystallization processes and affects the size of nanocrystals and the proportion of the nanocrystalline component in amorphous-nanocrystalline alloys. In this case, the prehistory of samples appeared to be of importance, namely, under what conditions the formation of the heterogeneous structure occurred: heating or deformation. The processes of crystallization under heating were studied in alloys of various compositions, having a homogeneous or heterogeneous amorphous structure. Comparative studies were carried out as follows [194]. The homogeneous amorphous phase was observed in alloys immediately after hardening, and the heterogeneous one was obtained by two methods: thermal treatment or deformation of the initial homogeneous amorphous phase. In these treatments, special control of the structural state of the samples was undertaken to ensure the formation of a heterogeneous amorphous structure rather than the beginning of crystallization. As a result, the following was established: in the *heterogeneous* phase obtained by deformation (HP/D), the nanocrystals formed were of a smaller size than in the heterogeneous amorphous phase obtained by thermal treatment (HP/T) (for example, 26 and 30 nm for the $Al_{87}Ni_8La_5$ alloy, respectively, 21 and 24 nm for the $Al_{87}Ni_8Gd_5$ alloy). The proportion of nanocrystals formed in HP/D was greater than for HP/T (25 and 20%, respectively, in the $Al_{87}Ni_8Y_5$ alloy). The size of nanocrystals also depends on the chemical composition: in the studied Al–Ni–*RE* (*RE* = La, Gd, Y) group of alloys, the largest nanocrystals formed in the amorphous alloy with lanthanum, and the smallest, in the alloy with yttrium. However, the most important fact discovered in these studies is that in all alloys during the crystallization of a *homogeneous* amorphous phase the proportion of nanocrystals was smaller than for the crystallization of a *heterogeneous* amorphous phase, and the size of the nanocrystals was noticeably greater. The results obtained testify to the possibility of affecting the amorphous phase structure in order to create nanostructures with the desired structural parameters under subsequent crystallization.

7. Conclusion

To conclude, we should note that the formation of nanostructures in metallic glasses depends on a variety of parameters. The crystallization mechanisms depend on both the chemical composition of the material and the state of the amorphous phase before the beginning of its decomposition, as well as the specific features of external actions. In the process of complex sequencing of phase transformations (homogeneous amorphous phase → nanoglass → metastable phases → equilibrium crystalline structure), materials with various structural parameters and, consequently, substantially different properties can form. The size and morphology

of nanocrystals and the fraction of the nanocrystalline component depend on whether the nucleation and growth of the crystals occur in a homogeneous or heterogeneous matrix and if the process is induced by thermal treatment or deformation. Combined treatments allow producing nanocrystalline materials with various structural characteristics. Many aspects of nanostructure formation remain unclear; however, the results of investigations performed have allowed a noticeable advancement towards creating nanomaterials with the proper physical and chemical properties.

This study was carried out within the State Assignment to the Institute of Solid State Physics of the Russian Academy of Sciences.

References

1. Xu J, Atzmon M *Appl. Phys. Lett.* **73** 1805 (1998)
2. Hebert R J et al. *J. Alloys Compd.* **434–435** 18 (2007)
3. Jiang W H, Atzmon M *Appl. Phys. Lett.* **86** 151916 (2005)
4. Jiang W H, Atzmon M *Scr. Mater.* **54** 333 (2006)
5. Allen D R, Folley J C, Perepezko J H *Acta Mater.* **46** 431 (1998)
6. Birringer R *Mater. Sci. Eng. A* **117** 33 (1989)
7. Abrosimova G E et al. *J. Mater. Sci.* **34** 1611 (1999)
8. Kulik T *J. Non-Cryst. Solids* **287** 145 (2001)
9. Louzguine-Luzgin D V, Inoue A *J. Nanosci. Nanotechnol.* **5** 999 (2005)
10. Kelton K F et al. *J. Non-Cryst. Solids* **317** 71 (2003)
11. Ramanujan R V, Du S W *J. Alloys Compd.* **425** 251 (2006)
12. Abrosimova G E, Aronin A S *Phys. Solid State* **50** 159 (2008); *Fiz. Tverd. Tela* **50** 154 (2008)
13. Abrosimova G E et al. *Phys. Solid State* **55** 1773 (2013); *Fiz. Tverd. Tela* **55** 1665 (2013)
14. Boucharat N et al. *Scr. Mater.* **53** 823 (2005)
15. Valiev R Z, Aleksandrov I V *Ob'emnye Nanostrukturnye Metallicheskie Materialy: Poluchenie, Struktura i Svoistva* (Bulk Nanostructured Metallic Materials: Preparation, Structure and Properties) (Moscow: Akademkniga, 2007)
16. Jiang W H, Atzmon M *Acta Mater.* **51** 4095 (2003)
17. Wilde G, Rösner H *Appl. Phys. Lett.* **98** 251904 (2011)
18. Csontos A A, Shiflet G J *Nanostruct. Mater.* **9** 281 (1997)
19. Abrosimova G, Aronin A *J. Alloys Compd.* **747** 26 (2018)
20. Pershina E et al. *Mater. Lett.* **134** 60 (2014)
21. Abrosimova G et al. *Mater. Lett.* **183** 131 (2016)
22. Aronin A et al. *J. Alloys Compd.* **715** 176 (2017)
23. Shechtman D et al. *Phys. Rev. Lett.* **53** 1951 (1984)
24. Kelton K F et al. *Phys. Rev. Lett.* **90** 195504 (2003)
25. Shen Y T et al. *Phys. Rev. Lett.* **102** 057801 (2009)
26. Saida J et al. *Appl. Phys. Lett.* **75** 3497 (1999)
27. Abrosimova G E et al. *Phys. Solid State* **46** 2191 (2004); *Fiz. Tverd. Tela* **46** 2119 (2004)
28. Abrosimova G E, Aronin A S, Serebraykov A V *Suppl. Trans. JIM* **20** 485 (1988)
29. Duwez P, Willens R H, Klement W (Jr.) *J. Appl. Phys.* **31** 1136 (1960)
30. Hermann H et al. *J. Non-Cryst. Solids* **317** 91 (2003)
31. Aronin A S et al. *Mater. Sci. Eng. A* **226–228** 536 (1997)
32. Yavari A R *Int. J. Rapid Solidif.* **2** 47 (1986)
33. Inoue A et al. *J. Mater. Sci. Lett.* **6** 194 (1987)
34. Yavari A R *Acta Metallurg.* **36** 1863 (1988)
35. Abrosimova G E et al. *J. Magn. Magn. Mater.* **203** 169 (1999)
36. Abrosimova G E, Aronin A S *J. Surf. Investig.* **9** 887 (2015); *Poverkhnost'. Rentgen. Sinkhrotron. Neitron. Issled.* (9) 27 (2015)
37. Gleiter H *Beilstein J. Nanotechnol.* **4** 517 (2013)
38. Ablesimov N E, Tsyurupa A G, Lipatov V G *Dokl. Akad. Nauk SSSR* **290** 1454 (1986)
39. Greer A L, in *Nanostructured Materials. Science and Technology* (NATO ASI Series, Vol. 50, Eds G-M Chow, N I Noskova) (Dordrecht: Kluwer Acad. Publ., 1998) p. 143
40. Foley J C, Allen D R, Perepezko J H *Scr. Mater.* **35** 655 (1996)
41. Schumacher P, McKay B J *J. Non-Cryst. Solids* **317** 123 (2003)
42. Mattern N et al. *Acta Mater.* **57** 903 (2009)
43. Han J H et al. *Acta Mater.* **66** 262 (2014)
44. Chou C-P P, Turnbull D *J. Non-Cryst. Solids* **17** 169 (1975)
45. Thompson C V, Spaepen F *Acta Metallurg.* **27** 1855 (1979)
46. Herold U, Köster U, in *Rapidly Quenched Metals III. Proc. of the 3rd Intern. Conf. on Rapidly Quenched Metals, Univ. of Sussex, Brighton, on 3–7 July, 1978* Vol. 1 (Ed. B Cantor) (London: Metals Society, 1978) p. 281
47. Cahn R W, in *Physical Metallurgy* Vol. 2 (Eds R W Cahn, P Haasen) (Amsterdam: North-Holland, 1983); Translated into Russian: in *Fizicheskoe Metallovedenie* Vol. 2 (Eds R W Cahn, P Haasen) (Moscow: Metallurgiya, 1987)
48. Scott M G, in *Amorphous Metallic Alloys* (Ed. F E Luborsky) (London: Butterworth-Heinemann, 1983) p. 144; Translated into Russian: in *Amorfnye Metallicheskie Splavy* (Ed. F E Luborsky) (Moscow: Metallurgiya, 1987)
49. Köster U, Herold U, in *Glassy Metals I. Ionic Structure, Electronic Transport, and Crystallization* (Topics in Applied Physics, Vol. 46, Eds H-J Güntherodt, H Beck) (Berlin: Springer-Verlag, 1981) p. 225; Translated into Russian: Köster U, Herold U, in *Metallicheskie Stekla* Vol. 1 *Ionnaya Struktura, Elektronnyi Perenos i Kristallizatsiya* (Eds H-J Güntherodt, H Beck) (Moscow: Mir, 1983)
50. Gutzow I, Toschev S, in *Advances in Nucleation and Crystallization of Glasses. Symp., April 26–28, 1971* (Eds L L Hench, S W Freiman) (Columbus, OH: American Ceramic Society, 1971)
51. Christian J W *The Theory of Transformations in Metals and Alloys: an Advanced Textbook in Physical Metallurgy* (International Series on Materials Science and Technology, Vol. 15) (Oxford: Pergamon Press, 1975); Translated into Russian: *Teoriya Prevrashchenii v Metallakh i Splavakh* Vol. 1 (Moscow: Mir, 1978)
52. Turnbull D, Cohen M H, in *Modern Aspects of the Vitreous State* Vol. 1 (Ed. J D Mackenzie) (London: Butterworth, 1960) p. 38
53. Köster U, Schünemann U, in *Rapidly Solidified Alloys. Processes, Structures, Properties, Applications* (Ed. H H Liebermann) (New York: M. Dekker, 1993) p. 303
54. Zener C *J. Appl. Phys.* **20** 950 (1949)
55. Aaron H B, Fainstein D, Kotler G R *J. Appl. Phys.* **41** 4404 (1970)
56. Greer A L *Acta Metallurg.* **30** 171 (1982)
57. Kelton K F, in *Solid State Physics* Vol. 45 (Eds H Ehrenreich, D Turnbull) (New York: Acad. Press, 1991) p. 75
58. Popov V V et al. *J. Non-Cryst. Solids* **356** 1344 (2010)
59. Tkatch V I et al. *J. Non-Cryst. Solids* **430** 108 (2015)
60. Tkatch V I *J. Non-Cryst. Solids* **351** 1658 (2005)
61. Ham F S *J. Phys. Chem. Solids* **6** 335 (1958)
62. Aaron H B, Fainstein D, Kotler G R *J. Appl. Phys.* **41** 4404 (1970)
63. Jacovkis D et al. *Acta Mater.* **52** 2819 (2004)
64. Clavaguera-Mora M T et al. *Prog. Mater. Sci.* **47** 559 (2002)
65. Vasiliev S V et al. *J. Alloys Compd.* **744** 141 (2018)
66. Kovalenko O V, Vasiliev S V, Tkatch V I *J. Non-Cryst. Solids* **518** 36 (2019)
67. Vasiliev S V, Parfenii V I, Tkatch V I *J. Alloys Compd.* **824** 153926 (2020)
68. Aronin A S, Abrosimova G E, Kir'yanov Yu V *Phys. Solid State* **43** 2003 (2001); *Fiz. Tverd. Tela* **43** 1925 (2001)
69. Yoshizawa Y, Oguma S, Yamauchi K *J. Appl. Phys.* **64** 6044 (1988)
70. Mehra M, Schulz R, Johnson W L *J. Non-Cryst. Solids* **61–62** 859 (1984)
71. Nagarajan T et al. *Hyperfine Interact.* **34** 491 (1987)
72. Pokatilov V S *Phys. Dokl.* **29** 234 (1984); *Dokl. Akad. Nauk SSSR* **275** 79 (1984)
73. Abrosimova G E, Aronin A S *Int. J. Rapid Solidif.* **6** 29 (1991)
74. Abrosimova G E et al. *Fiz. Met. Metalloved.* **62** 496 (1986)
75. Herold U, Köster U *Z. Metallk.* **69** 326 (1978)
76. Abrosimova G E et al. *Sov. Phys. Solid State* **30** 822 (1988); *Fiz. Tverd. Tela* **30** 1424 (1988)
77. Spriano S et al. *Phil. Mag. B* **76** 529 (1997)
78. Xing L Q et al. *Appl. Phys. Lett.* **74** 664 (1999)
79. Abrosimova G, Aronin A, Ignatieva E *Mater. Sci. Eng. A* **449–451** 485 (2007)
80. Abrosimova G et al. *Mater. Lett.* **219** 97 (2018)
81. Abrosimova G E, Aronin A S, Volkov N A *Phys. Solid State* **61** 1294 (2019); *Fiz. Tverd. Tela* **61** 1352 (2019)
82. Volkov N, Abrosimova G, Aronin A *Mater. Lett.* **265** 127431 (2020)

83. Skryshevskii A F *Strukturnyi Analiz Zhidkostei i Amorfnykh Tel* (Structural Analysis of Liquids and Amorphous Bodies) (Moscow: Vysshaya Shkola, 1980)
84. Nemoshkalenko V V et al. *Amorfnye Metallicheskie Splavy* (Amorphous Metal Alloys) (Exec. Ed. V V Nemoshkalenko) (Kiev: Naukova Dumka, 1987)
85. Bhatia A B, Thornton D E *Phys. Rev. B* **2** 3004 (1970)
86. Mattern N et al. *Acta Mater.* **50** 305 (2002)
87. Cheng Y Q, Ma E *Prog. Mater. Sci.* **56** 379 (2011)
88. Louzguine-Luzgin D V et al. *J. Appl. Phys.* **110** 043519 (2011)
89. Louzguine-Luzgin D V et al. *Intermetallics* **122** 106795 (2020)
90. Hirata A et al. *Nat. Mater.* **10** 28 (2011)
91. Abrosimova G E *Phys. Usp.* **54** 1227 (2011); *Usp. Fiz. Nauk* **181** 1265 (2011)
92. Chen H S, Turnbull D *Acta Metallurg.* **17** 1021 (1969)
93. Mak A, Samwer K, Johnson W L *Phys. Lett. A* **98** 353 (1983)
94. Naudon A, Flank A M *J. Non-Cryst. Solids* **61–62** 355 (1984)
95. Terauchi H et al. *J. Phys. Soc. Jpn.* **52** 3454 (1983)
96. Osamura K, Ochiai S, Takayama S *J. Mater. Sci.* **19** 1917 (1984)
97. Abrosimova G E et al. *Phys. Solid State* **40** 1264 (1998)
98. Osamura K et al. *Colloid Polymer Sci.* **259** 677 (1981)
99. Abrosimova G, Aronin A *Rev. Adv. Mater. Sci.* **50** 55 (2017)
100. Abrosimova G E, Aronin A S *J. Surf. Investig.* **9** 134 (2015); *Poverkhnost. Rentgen. Sinkhrotron. Neitron. Issled.* (2) 28 (2015)
101. Abrosimova G, Aronin A, Budchenko A *Mater. Lett.* **139** 194 (2015)
102. Liebermann H H, Graham C, Flanders P *IEEE Trans. Magn.* **13** 1541 (1977)
103. Naka M, Masumoto T, Chen H S *J. Physique Colloques* **41** C8-839 (1980)
104. Chen H S *Mater. Sci. Eng.* **26** 79 (1976)
105. Mu J et al. *Adv. Eng. Mater.* **11** 530 (2009)
106. Yang B J et al. *Phil. Mag.* **90** 3215 (2010)
107. Du S et al. *Mater. Design* **47** 358 (2013)
108. Chunchu V J, Markandeyulu G *J. Appl. Phys.* **113** 17A321 (2013)
109. Doi K, Ayano T, Kawamura K *J. Non-Cryst. Solids* **34** 405 (1979)
110. Gerling R, Wagner R *Scr. Metallurg.* **16** 963 (1982)
111. Gerling R, Wagner R *J. Nucl. Mater.* **107** 311 (1982)
112. Gerling R, Schimansky F P, Wagner R *J. Non-Cryst. Solids* **61–62** 919 (1984)
113. Wagner R, Gerling R, Schimansky F P *J. Non-Cryst. Solids* **61–62** 1015 (1984)
114. Meng F et al. *Appl. Phys. Lett.* **101** 121914 (2012)
115. Tong Y et al. *Acta Mater.* **86** 240 (2015)
116. Dmowski W et al. *Acta Mater.* **58** 429 (2010)
117. Guo W, Yamada R, Saida J *Intermetallics* **93** 141 (2018)
118. Ketov S V et al. *Nature* **524** 200 (2015)
119. Hufnagel T C *Nat. Mater.* **14** 867 (2015)
120. Kang S J et al. *J. Alloys Compd.* **795** 493 (2019)
121. Abrosimova G et al. *Mater. Lett.* **240** 150 (2019)
122. Abrosimova G et al. *J. Non-Cryst. Solids* **528** 119751 (2020)
123. Serbena F C, Zanotto E D *J. Non-Cryst. Solids* **358** 975 (2012)
124. Aronin A S, Louzguine-Luzgin D V *Mech. Mater.* **113** 19 (2017)
125. Lewandowski J J, Greer A L *Nat. Mater.* **5** 15 (2006)
126. Csontos A A, Shiflet G J *Nano Struct. Mater.* **9** 281 (1997)
127. Georgarakis K et al. *Appl. Phys. Lett.* **93** 031907 (2008)
128. Rösner H et al. *Ultramicroscopy* **142** 1 (2014)
129. Schmidt V et al. *Phys. Rev. Lett.* **115** 035501 (2015)
130. Greer A L, Cheng Y Q, Ma E *Mater. Sci. Eng. R* **74** 71 (2013)
131. Gunderov D et al. *Rev. Adv. Mater. Sci.* **25** 58 (2010)
132. Gunderov D V et al. *Intermetallics* **66** 77 (2015)
133. Gunderov D V et al. *Vestn. Bashkirskogo Univ.* **20** 403 (2015)
134. Churakova A et al. *Acta Metallurg. Sinica* (*Engl. Lett.*) **28** 1230 (2015)
135. Wang X D et al. *Scr. Mater.* **64** 81 (2011)
136. Meng F et al. *Appl. Phys. Lett.* **101** 121914 (2012)
137. Perepezko J H, Hebert R J *JOM* **54** 34 (2002)
138. Abrosimova G E et al. *Phys. Solid State* **52** 1892 (2010); *Fiz. Tverd. Tela* **52** 1763 (2010)
139. Abrosimova G E, Aronin A S *Phys. Solid State* **59** 2248 (2017); *Fiz. Tverd. Tela* **59** 2227 (2017)
140. Abrosimova G E, Aronin A S, Shirnina D P *Fiz. Tekh. Vys. Davl.* **23** (1) 90 (2013)
141. Yokoyama Y, Yamasaki T, Inoue A *Rev. Adv. Mater. Sci.* **18** 131 (2008)
142. Abrosimova G et al. *Mater. Lett.* **97** 15 (2013)
143. Wang K et al. *Acta Mater.* **56** 2834 (2008)
144. Abrosimova G et al. *Phys. Solid State* **53** 229 (2011); *Fiz. Tverd. Tela* **53** 215 (2011)
145. Aronin A S, Abrosimova G E *Mater. Lett.* **83** 183 (2012)
146. Glezer A M, Manaenkov S E, Permyakova I E *Bull. Russ. Acad. Sci.* **71** 1702 (2007); *Izv. Ross. Akad. Nauk. Ser. Fiz.* **71** 1764 (2007)
147. Abrosimova G et al. *Mater. Lett.* **183** 131 (2016)
148. Boucharat N et al. *J. Alloys Compd.* **434–435** 252 (2007)
149. Eckert J et al. *Rev. Adv. Mater. Sci.* **18** 169 (2008)
150. Greer A L *Mater. Sci. Eng. A* **304–306** 68 (2001)
151. Glezer A M *Phys. Usp.* **55** 522 (2012); *Usp. Fiz. Nauk* **182** 559 (2012)
152. Andrievski R A, Glezer A M *Phys. Usp.* **52** 315 (2009); *Usp. Fiz. Nauk* **179** 337 (2009)
153. Glezer A M et al. *Deform. Razrushenie Mater.* (4) 2 (2012)
154. Glezer A M et al. *Izv. Ross. Akad. Nauk Ser. Fiz.* **73** 1302 (2009)
155. Shao H et al. *J. Alloys Compd.* **548** 77 (2013)
156. Lee M H et al. *Scr. Mater.* **62** 678 (2010)
157. Abrosimova G E, Aronin A S *Phys. Solid State* **44** 1003 (2002); *Fiz. Tverd. Tela* **44** 961 (2002)
158. Valiev R Z et al. *J. Metastable Nanocryst. Mater.* **22** 21 (2004)
159. Boltynjuk E V et al. *J. Alloys Compd.* **747** 595 (2018)
160. Dubach A, Dalla Torre F H, Löffler J F *Phil. Mag. Lett.* **87** 695 (2007)
161. Abrosimova G, Aronin A *Mater. Lett.* **206** 64 (2017)
162. Hall E O *Proc. Phys. Soc. B* **64** 747 (1951)
163. Petch N J *J. Iron Steel Inst.* **174** 25 (1953)
164. Lu K *Mater. Sci. Eng. R* **16** 161 (1996)
165. Liu X D, Wang J T, Ding B Z *Scr. Metallurg. Mater.* **28** 59 (1993)
166. Cremashi V et al. *J. Mater. Res.* **15** 1936 (2000)
167. Ohta M, Yoshizawa Y *Appl. Phys. Lett.* **91** 062517 (2007)
168. Suzuki K et al. *Mater. Trans. JIM* **32** 93 (1991)
169. Makino A, Inoue A, Masumoto T *Nanostruct. Mater.* **6** 985 (1995)
170. Hono K et al. *Acta Metall. Mater.* **40** 2137 (1992)
171. Herzer G *IEEE Trans. Magn.* **30** 4800 (1994)
172. Kraus L et al. *J. Magn. Magn. Mater.* **112** 275 (1992)
173. Hofmann B, Kronmüller H *Nanostruct. Mater.* **6** 961 (1995)
174. Nemoskalenko V et al. *Metallofiz. Nov. Tekhnol.* **20** (11) 29 (1998)
175. Hono K *Prog. Mater Sci.* **47** 621 (2002)
176. Herzer G *J. Magn. Magn. Mater.* **294** 99 (2005)
177. Flohrer S et al. *Acta Mater.* **54** 4693 (2006)
178. Herzer G, Budinsky V, Polak C *J. Phys. Conf. Ser.* **266** 012010 (2011)
179. Azuma D et al. *J. Appl. Phys.* **113** 17A339 (2013)
180. Yoshizawa Y, Yamauchi K *Mater. Sci. Eng. A* **133** 176 (1991)
181. Yoshizawa Y et al. *Scr. Mater.* **48** 863 (2003)
182. Agudo P, Vázquez M *J. Appl. Phys.* **97** 023901 (2005)
183. Chau N et al. *J. Magn. Magn. Mater.* **303** e415 (2006)
184. Muraca D et al. *J. Magn. Magn. Mater.* **320** 1639 (2008)
185. Bayri N et al. *J. Non-Cryst. Solids* **355** 12 (2009)
186. Yan M et al. *J. Alloys Compd.* **505** 264 (2010)
187. Lu W et al. *J. Magn. Magn. Mater.* **322** 2935 (2010)
188. Balcerski J et al. *Vacuum* **83** (Suppl. 1) S182 (2009)
189. Gheiratmand T et al. *J. Alloys Compd.* **582** 79 (2014)
190. Shivaee H A et al. *Thermochim. Acta* **575** 64 (2014)
191. Herzer G, in *Handbook of Magnetic Materials* Vol. 10 (Eds K H J Buschow) (Amsterdam: North-Holland, 1997) p. 415
192. Aronin A et al. *Rev. Adv. Mater. Sci.* **46** 53 (2016)
193. Abrosimova G E et al. *Scr. Metallurg.* **14** 967 (1980)
194. Aronin A et al. *J. Alloys Compd.* **715** 176 (2017)
195. Hóbor S et al. *Rev. Adv. Mater. Sci.* **18** 590 (2008)
196. Kovács Zs et al. *Rev. Adv. Mater. Sci.* **18** 593 (2008)
197. Henits P, Kovács Zs, Révész Á *Rev. Adv. Mater. Sci.* **18** 597 (2008)
198. Shirnina D P, Abrosimova G E, Aronin A S *Dizain Mater. Tekhnol.* (3(18)) 80 (2011)